

EU Horizon program: Horizon-CL4-2021-TWIN Transition
Reducing environmental footprint, improving circularity in extractive and
processing value chains (IA)
Refractory Sorting Using Revolutionizing Classification Equipment
Grant Agreement No 101058310

WP 4 Preparation for sorting
D4.1 Comprehensive fractional class analysis
and comminution investigations

ReSoURCE

Project Reference No	101058310
Deliverable	D4.1 Comprehensive fractional class analysis and comminution investigation
Work Package	WP4
Type	R
Dissemination Level	PU
Date	August 2024
Status	Final version
Editor(s)	Karl Friedrich, Simone Neuhold, Stefan Heid, Alexander Leitner, Helmut Flachberger, Kristin Sjøiland, Chandana Ratnayake
Contributor(s)	MUL, RHIM, SINTEF
Reviewers	All partners
Document description	This deliverable reports about the fractional class analysis and comminution investigations of refractory bricks.

Document revision history

Version	Date	Modification introduced	
		Modification reason	Author
V0.1	10.05.2024	1 st version	Karl Friedrich, Simone Neuhold, Stefan Heid, Alexander Leitner, Helmut Flachberger, Kristin Søyland, Chandana Ratnayake
V1.0	19.07.2024	2 nd version	Karl Friedrich, Simone Neuhold, Stefan Heid, Alexander Leitner, Helmut Flachberger, Kristin Søyland, Chandana Ratnayake
V2.0	01.08.2024	3 rd version	Karl Friedrich, Simone Neuhold, Stefan Heid, Alexander Leitner, Helmut Flachberger, Kristin Søyland, Chandana Ratnayake
V3.0	06.08.2024	4 th version	Karl Friedrich, Simone Neuhold, Stefan Heid, Alexander Leitner, Helmut Flachberger, Kristin Søyland, Chandana Ratnayake
V4.0	13.08.2024	5 th version	Karl Friedrich, Simone Neuhold, Stefan Heid, Alexander Leitner, Helmut Flachberger, Kristin Søyland, Chandana Ratnayake

Executive Summary

This deliverable reports on the comprehensive fractional class analysis and comminution investigations of secondary refractory materials. The primary goal was to evaluate and identify the most effective comminution technologies for processing spent refractory bricks to facilitate subsequent sorting and recycling processes. The work reported in this deliverable refers to ReSoURCE project ([Resource - Refractory Sorting Using Revolutionizing Classification Equipment](#)) in the framework of WP4 – Preparation for sorting.

The study involved the comminution of various types of secondary refractory materials to a size of less than 40 mm after pre-crushing them to an output size of less than 120 mm. Different crushers, including jaw crushers, cone crushers, and impact crushers, were used under defined conditions. The results indicated that jaw and cone crushers were most effective in producing particles with suitable length-to-width ratios for sorting by picker robots, while minimizing the generation of fines (<5 mm).

The second objective was to assess the most suitable comminution technology for achieving the liberation of particles in refractory bricks, giving several advantages for sorting within Demonstrator B. Four comminution technologies were tested: jaw crushers, cone crushers, impact crushers, and electrodynamic fragmentation (EDF). The experiments demonstrated that jaw and cone crushers were the most effective in enriching elements (Mg and C for MgO-C, Fe and Al for Hercynite) in specific particle size fractions. EDF showed limited effectiveness in producing significant elemental enrichment or particle comminution.

This deliverable provides valuable insights and practical recommendations for the industrial application of comminution technologies in refractory material recycling, contributing to the overall objectives of the ReSoURCE project.

Table of Contents

1	Introduction	5
2	Theory of comminution	6
2.1	Jaw crusher	7
2.2	Cone crusher	7
2.3	Impact crusher	8
2.4	Electrodynamic fragmentation (EDF)	9
3	Materials and Methods	11
3.1	Material description	11
3.2	Coarse comminution, <120 mm	12
3.3	Conventional and alternate comminution, <5 mm	18
3.4	Fractional class analysis	18
4	Results and Discussion	22
4.1	Coarse comminution, <120 mm	22
4.2	Conventional and alternate comminution, <4 mm	29
4.3	Fractional class analysis	36
5	Conclusion	40
5.1	Coarse comminution, <120 mm	40
5.2	Conventional and alternate comminution, <4 mm	41
5.3	Fractional class analysis	41
5.4	Impact on ReSoURCE	42
6	References	43
7	List of figures	44
8	List of tables	46
9	Appendix	47

1 Introduction

The comprehensive fractional class analysis of the different spent refractory material samples from task 3.3 will serve to determine the phase composition relevant for processing, intergrowth ratios, and identification of usable property differences for subsequent separation.

Finding the most suitable comminution technology is an important requirement for efficient separation. The main challenge lies in the wide range of different used refractory products which have different comminution behaviors. Maximizing fractions that are amenable to processing by sensor-based sorting will be the priority.

The objectives of this deliverable refer to the particle size of the fraction to be treated:

1. Evaluate the most suitable crushing technology for the separation in the first crushing step (Acronym: Coarse comminution, <120 mm)
2. Evaluate the most suitable crushing technology to get individual particles of refractory bricks (Acronym: Conventional and alternate comminution, <5 mm)

In the first step the breakout material needs to be crushed to a particle size <120 mm (Coarse comminution, <120 mm). Larger fragments would exceed the upper weight limit of the robots used for ejection. Furthermore, it is important that the fines (<5 mm) are reduced to a minimum during this first comminution process, as this unsorted fraction will end up in low-value products only. It is therefore crucial to maximize the share of material in a processable particle size range for subsequent sorting in Demonstrator A to increase the overall efficiency of the plant. Another factor, which has an impact on the performance of the plant, is that the surface of the crushed particles is beneficial for the sensor classification.

The first comminution step will be done with a conventional aggregate such as a jaw crusher, cone crusher or impact crusher.

The initial comminution step generates material that will be separated into three fractions based on particle size. Material in the particle size range 60–120 mm will be classified with sorting robots, while the fraction 5–60 mm will be sorted with an air ejection system. Sorting of the fine fraction <5 mm is not covered in work package 4, sorting methods for this fraction are evaluated in work package 7.

Following the sorting of both fractions, the next step involves achieving a particle size of <5 mm as this is the typical size range to be directly reused in refractory production. This can either be achieved by further conventional comminution or by novel methods such as electro dynamic fragmentation. The main goal is to achieve well liberated particles with as little conglomerates as possible. The idea is to reuse fully- or well-liberated particles in new refractory bricks being beneficial for refractory quality, as they should closely match the quality of primary raw materials.

EDF is an emerging technology known from mining and concrete industry, which could be an innovative solution for refractories to liberate initial raw materials from their matrix to increase the quality of recycling material used in refractories. EDF is a material selective comminution for solid material compounds and is therefore expected to be a suitable alternative to traditional approaches as mineral liberation should mainly take place at phase interfaces. Consequently, it offers perspectives for developing a new generation of environmentally and economically viable material processing technologies. [1]

2 Theory of comminution

The purpose of comminution is to reduce the particle size of solid materials, thereby modifying their dispersity. The specific goals of comminution, however, depend on subsequent processing steps or the intended further use of the material. The degree of dispersion can be defined by a specific particle size or particle shape distribution, surface enlargement, liberating material components or obtaining structural changes and chemical reactions. [2]

The comminution process itself is related to external stress on a solid material which is applied manually at interfaces between mineral particles and comminution equipment (e.g., working surface of a crusher). For this purpose, the load intensity and load velocity can be varied independently. [2]

If the applied stress is higher than the binding forces, a crack formation at particle boundaries inside the mineral material is initialized. Mechanical stress can be applied by compression, shearing, strike – all these types are related to processing within two surfaces (see Figure 1). Compressive strength is typical for crushing equipment (e.g., jaw crusher, cone crusher) with relatively low load velocities (up to 5 m/s). Shearing proceeds if two working surfaces fulfil a relative movement towards each other, where the crushed material is located within these two surfaces. Strike is a type of compressive strength at high load velocities (higher than 5 m/s). Impact stress is applied by mechanical load at a working surface - load intensity and load velocity are interdependent (coarse and middle comminution with loading velocities up to 20–60 m/s). [2]

Comminution equipment is categorized by particle size range (coarse 100–1000 mm, middle 10–100 mm, fine 10–0.1 mm, finest 0.1–0.001 mm) and strength characteristics (hard e.g., slags, semi-hard e.g., limestone, soft e.g. clays). [2]

For processing spent refractories, the primary objectives of comminution are to achieve a specific particle size and shape distribution and to enhance mineral liberation. This facilitates subsequent processing steps, such as manual or automated sorting.

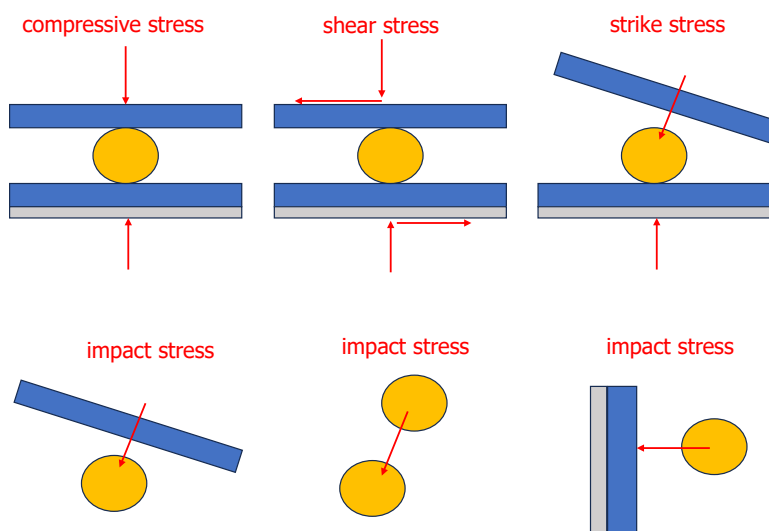


Figure 1: Principles of different comminution types [2]

2.1 Jaw crusher

Jaw crushers (Figure 2) are typically used for hard to semi-hard materials which are loaded by compressive strength in the process area. [2]

Operation mode of a jaw crusher is defined by one fixed and one movable crusher jaw – the material is placed within these two jaws. Machine safety is applied by slipping clutch, shear bolts and other elements which are placed between flywheels and jaws and can prevent them of kinetic forces. Jaw crushers are characterized by a comminution ratio of six to nine which means feeding size is six to nine times higher than the expected particle size. The stroke rate defines the success of comminution – a low stroke rate led to a high packing density within the crushing operation area. If the stroke rate is too high, the retention time is too short and prevents the material from sliding along the operation area. Both cases led to performance losses. Therefore, the stroke rate is typically between 180 and 250 min^{-1} whereas the stroke path at the discharge gap is between 15–25 mm (depending on gap width). [2]

To obtain fragmentation the jaws are designed with crusher teeth – the jaw inclination must be lower than the friction angle (jaw inclination increases with comminution resistance). Industrially employed are single- and double-toggle jaw crushers as well as impact jaw crushers. [2]

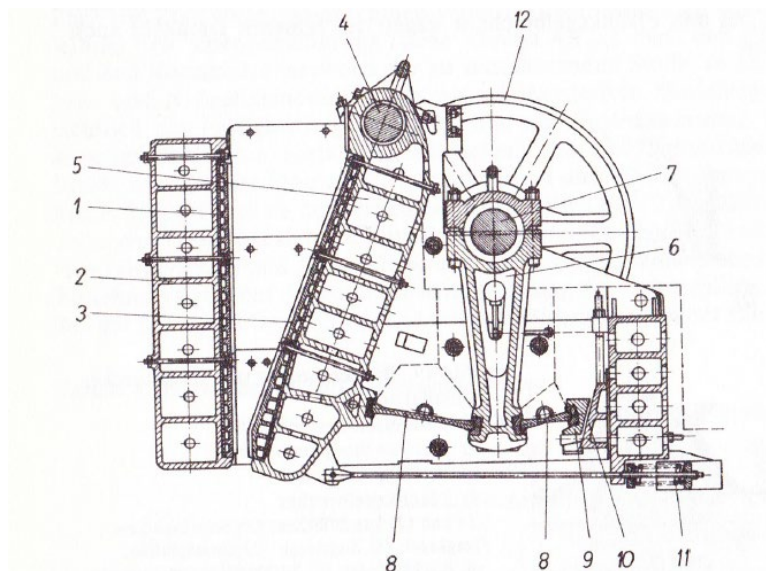


Figure 2: Principles of jaw crusher [2]

2.2 Cone crusher

Cone crushers (Figure 3) are like jaw crushers typically used for hard to semi-hard materials – whereby it is differentiated between gyratory and Symons crusher, both characterized by a ring-shaped operation area. Symons crushers are characterized by higher rotational speed – as a result, strike stress is the main factor to be considered for this equipment. Gyratory crushers exhibit a comminution ratio ranging from five to eight, with a comminution effect comparable to that of a toggle jaw crusher. Conversely, Symons crushers achieve a comminution ratio up to 15, performing similarly to an impact crusher. [2]

The operation area of a gyratory crusher is defined by a hollow-cone shaped crushing shell and a crushing cone. Crushing is accomplished by feeding the material in the converging space between crushing shell and crushing cone. The gap width at the bottom of the hollow-cone defines the particle size of the comminution product. [2]

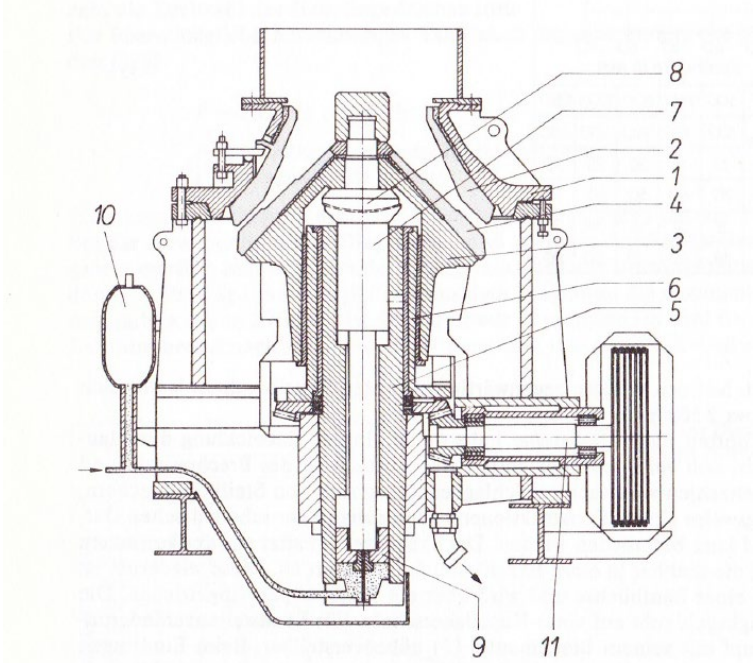


Figure 3: Principles of cone crusher [2]

2.3 Impact crusher

Impact crushers (Figure 4) are used for coarse and semi-coarse feeding materials. A fast-rotating impact drum accelerates the material towards flapper plates in the operating crushing area – these fixed plates are feeding the material back to the rotating impact drum. [2]

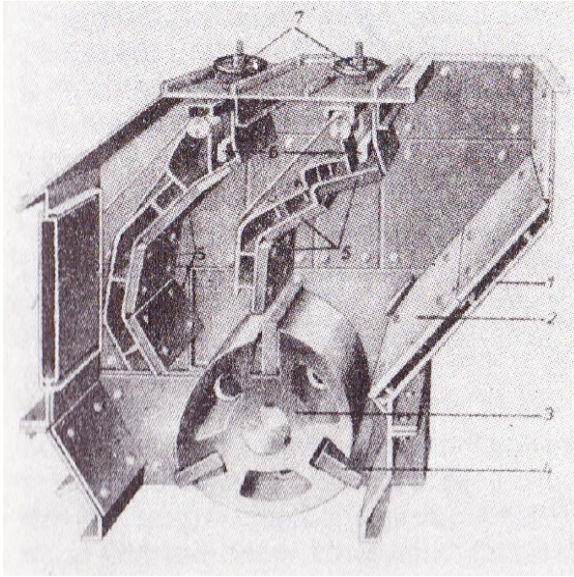


Figure 4: Principles of impact crusher [1]

2.4 Electrodynamic fragmentation (EDF)

The overall aim of EDF is to efficiently achieve selective liberation from complex matrices. The fundamental issue in the recycling business is the wide range of composite materials, which necessitate liberation to separate them subsequently. [3]

EDF is a selective crushing technology of solid materials using high-voltage pulsed power discharges realized as a wet batch process. When the feed material exhibits significant differences in relative permittivity, the electric pulse penetrates the boundaries in the particle matrix. Refractories are generally composed of various components, mainly high refractory oxides, such as MgO, Al₂O₃ or SiO₂. Due to different electrical properties of the individual constituents, EDF might be suitable to achieve better liberated particles with less conglomerates than a conventional comminution technology. The main components of the EDF lab equipment (Figure 5) at MUL – provided by the company selFrag – are the high voltage power supply, generator, high voltage working electrodes, mobile process vessel, lifting platform, and control panel. A Marx generator is required to produce the required high voltage. [3] The discharge voltage (90–200 kV), electrode gap (10–40 mm), pulse rate (1–5 Hz), and pulse count (1–1000) are adjustable. The lab unit is designed for sample sizes of up to 1 kg. [4]



Figure 5: EDF lab equipment at MUL [5]

Comminution mechanism

A high pulse rate, measured in pulses per second, facilitates the generation of a discharge. The electrode gap describes the volume of the processing zone between the electrodes, which limits the number of particles that can be loaded. The voltage gradient (in kV mm^{-1}) influences the discharge ratio. The device generates a high voltage of 90–200 kV and discharges it within a few microseconds, generating a pulse which penetrates the particles, inducing stress and therefore creating micro-cracks along the natural phase boundaries (Figure 6). [6]

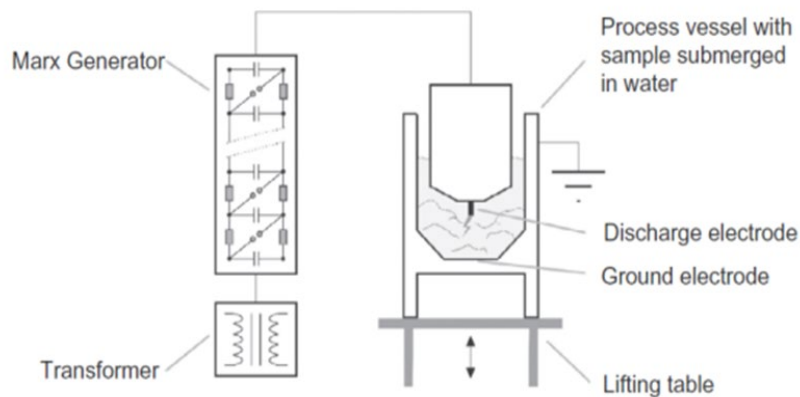


Figure 6: selfFrag lab device's schematic [7]

Comminution Process

The sample is placed in the process vessel which is equipped with electrodes at the bottom and filled with a fixed amount of water. The container is moved by the lifting table to align with the top electrode, allowing a voltage discharge to occur between the two electrodes. When the sample is large, a higher pulse voltage and a wider distance between sensors are usually applied. [5]

A cylindrical plastic drum is attached to the bottom of the metal mesh sieve with a provided aperture. The fine particles smaller than the mesh size pass through the sieve and are collected in the container below, while the coarse particles remain on the screen. The cut-point can be adjusted using interchangeable sieves. [8]

After comminution, the water residue is drained or collected separately for further analysis.

Disadvantages and advantages of EDF

The number of samples processed per batch is very limited, making the process inefficient when dealing with large quantities of material. [5]

After each experiment, the fragments above and underneath the screen must be collected. If the sample size and mass are too small, the pulse voltage and electrode spacing must be decreased during the experiment to avoid failure. To some extent, it limits the analysis of certain samples and is not always suitable. [5] Being a wet process, subsequent drying of the material would cause additional processing costs.

The EDF lab has the following advantages compared to typical mechanical comminution technology: [8]

- Dust-free: comminution takes place in heated water, and the resulting powder is dispersed in the water. The absence of dust considerably enhances the working environment for sample comminution.
- Low noise: There is no significant noise pollution caused by this process.
- EDF does not destroy the crystals and therefore differs from conventional mechanical comminution technologies. Fracturing particles at their boundaries and other weak points preserves their internal structure and prevents overgrinding.

3 Materials and Methods

In the following section, the material is described and the methods for the objectives “Coarse comminution, <120 mm” and “Conventional and alternate comminution, <5 mm” are elucidated.

3.1 Material description

Refractory products find applications in high-temperature industrial processes, including steel, cement, and glass production. The refractory lining is designed to protect critical process units such as furnaces and hot metal ladles against chemical, mechanical and thermal stress and is tailored for specific applications. After end-of-life, the lining is dismantled at the e.g., steel or cement production site, whereby a mixing of products and the generation of fine particles are unavoidable. Furthermore, the dismantling process results in unpredictable particle size distributions (PSD) and adhesions (e.g., slag or clinker) cannot be removed completely.

In the ReSoURCE project, focus is set on spent refractories from steel casting ladles (SCL) and cement rotary kilns (CRK) with the following main brick types: magnesia-based carbon bonded bricks and alumina-based carbon bonded bricks for SCL; magnesia spinel burned bricks (iron rich or iron poor) for CRK (see D1.1). For the first subobjective “Coarse comminution, <120 mm” (described in chapter 1) RHIM provided pre-sorted and pre-commuted (<80 mm) breakout material from the cement and the steel industry. In total 3000 kg of the sorting classes “Hercynite” (iron rich magnesia spinel bricks) and “MgO-C” (magnesia-based carbon bonded bricks) were sampled and crushed after manual sorting at MIRECO site in Mitterdorf, Austria. In addition, 50 kg of main raw materials used in magnesia carbon and magnesia spinel bricks were provided.

For the second subobjective “Conventional and alternate comminution, <5 mm” (described in chapter 1) approximately 30 kg of the same sorting classes, i.e., “MgO-C” and “Hercynite” but from different feedstocks compared to the samples provided for “Coarse comminution, <120 mm” were sampled and crushed (<40 mm) at MIRECO site in Mitterdorf, Austria.

Figure 7 shows an example of the initial PSD, i.e., the size distribution of spent refractory material as received for manual sorting for feedstock CRK1. The data “hand sorting >80 mm” refers to 99 brick samples, hand sorted and measured at RHIM after representative sampling, the data “sieving 0–5 mm” refers to sieve analyses of 1.3 tons of material at RHIM. The analyses are based on representative samples taken for project ReSoURCE (see D1.1, D1.2 and D3.3).

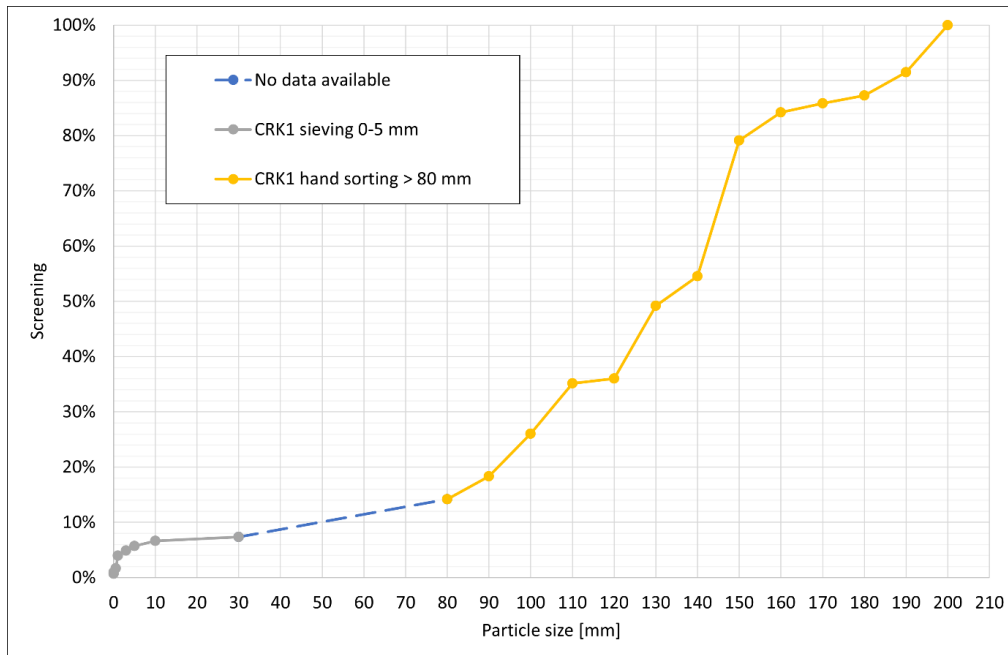


Figure 7: Initial particle size distribution of cement rotary kiln breakout material (CRK1).

3.2 Coarse comminution, <120 mm

The technical facility trials for the coarse comminution took place at the recycling plant of RHI Magnesita GmbH (MIRECO site in Mitterdorf, Sankt Barbara im Mürztal, Austria) and ARP – Aufbereitungs, Recycling und Prüftechnik GesmbH in Leoben, Austria. Furthermore, laboratory tests were conducted at Technology Center of RHI Magnesita GmbH and Montanuniversität Leoben, both situated in Leoben, Austria.

Preprocessing

The preselection of investigated material was defined within the work group of project package “preparation for sorting”. Therefore, different types of refractories have been reviewed since– five of these different input materials for recycling plant Mitterdorf were analyzed in detail. Refractory type, origin, dimensions, mass and raw densities on 50 individual samples for each input material were documented in WP 1.

The used refractories were common out-break materials from the cement and steel industry, typically handled in standard processing units in recycling plant Mitterdorf – two samples were of Hercynite and one of MgO-C. The dimensions of used bricks were up to 750 mm in length (mean 140–200 mm), up to 250 mm in width (mean 100–150 mm) and up to 525 mm in height (mean 90–320 mm).

To guarantee a range of material varieties and their different material characteristics, following types of spent refractories were preselected for industrial trials based on preceding works and availability (amount of waste, relevance for recycling efforts and waste purity) for industrial trials:

- Hercynite-based used refractories (two samples of different origins, CRK)
- MgO-C-based spent refractories (one sample, SCL)

The various out-break materials were properly stored in big bags (volume 1 m³). For the comminution process, refractories were reloaded into wheel loader shovel, whence the material was fed in a mobile jaw crusher. The comminution product was collected at the end of the jaw crusher’s conveyor belt and

filled into further big bags (volume 1 m³). The crushing process itself was continuous without pre-screening, the desired particle size was smaller than 120 mm (gap width of jaw crusher).

Following samples were prepared for further coarse comminution trials:

- Sample A (Hercynite): 1000 kg
- Sample B (Hercynite): 800 kg
- Sample C (MgO-C): 1379 kg

Preselecting comminution equipment for industrial trial

The selection of crushing equipment for further upscaling crushing trials was done at (ARP) in Leoben.

The aim of this work package was to compare different conventional comminution aggregates – the trial goal was the reduction of particle size (based on preprocessed material <120 mm) with producing as little fines (<5 mm) as possible. The final selection of the most appropriate comminution aggregate for the defined recycling task was therefore based on particle size distributions.

At ARP following crushing types were available: jaw crusher, cone crusher and impact crusher. With these three types it was planned to implement a pre-selecting step on a small level and to upscale it on a second step for higher testing volumes.

The prepared samples of used refractories (sample A, B and C, see Figure 8) were transferred from recycling plant Mitterdorf to ARP in Leoben, where a first pre-testing of this material and evaluation of crushing procedure was done. With this knowledge pre-settings for the different crushing equipment were predefined by testing gap widths between 40–50 mm.



Figure 8: sample A (Hercynite), sample B (Hercynite) and sample C (MgO-C), from left to right.

To define the most appropriate machinery settings, small amounts of subsamples (about 30–40 kg each) were preselected manually of each sample big bag – only particles bigger than 40 mm were used for this process step. The subsamples were fed manually at different crushing equipment.

The crushed products were sieved manually and based on the derived particle size distribution the crushing result was evaluated and machinery settings adjusted accordingly.

Following settings were varied to optimize the crushing results (producing as little fines <5 mm as possible):

- Jaw crusher: 1 setting (gap width 40 mm)
- Cone crusher: 2 settings with varied gap width (40 mm vs. 46 mm)
- Impact crusher: 2 settings with varied amplitude (50 Hz vs. 40.30 Hz) and fixed gap width (40 mm)

At the end all crushed products were sieved manually into five mass fractions (>40 mm, 20–40 mm, 10–20 mm, 5–10 mm, <5 mm). Particle shape distributions of fractions >10 mm were analyzed in laboratory (see green highlighted fractions in Figure 9).

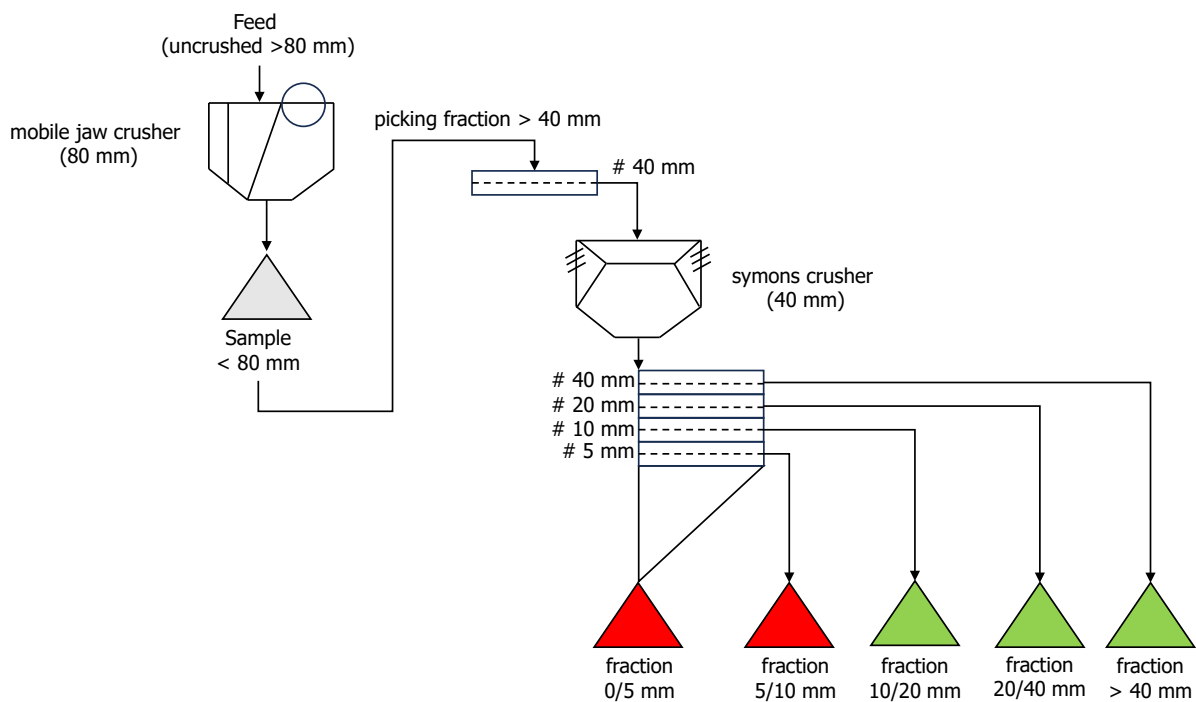


Figure 9: Preselecting comminution equipment - Flowsheet cone crusher.

Technical facility trials on industrial scale

Industrial comminution tests with cone crusher were conducted at ARP in Leoben.

Based on the experience from pre-selecting step, the cone crusher was evaluated as the most appropriate crushing equipment for further crushing trials with higher mass loads. A circular comminution process with refeeding mass fraction >40 mm was installed (Figure 10).

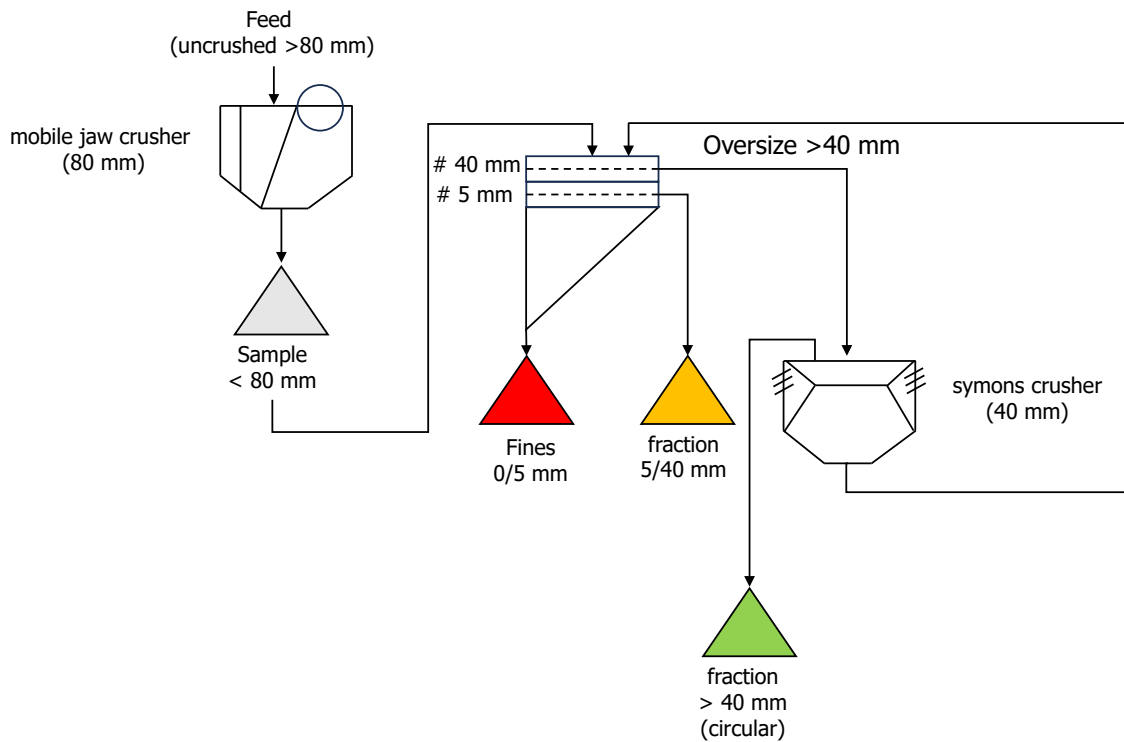


Figure 10: Industrial comminution equipment - Flowsheet cone crusher

To avoid over-crushing and therefore falsification of material comminution behavior, samples (A, B and C) were sieved with a circular vibratory screen at 5 mm and 40 mm (Figure 11). Only mass fraction >40 mm was used for further comminution – other fractions (5/40 mm, <5 mm) were stored in big bags and their mass was documented. Particles >40 mm not processable by the Symons crusher were used for further particle shape analysis. These fractions can be seen as “circular load”, which refers to particles not crushed by the cone crusher as they were blocking the ring gap during comminution operation (see Figure 12). Mass portions which were settling at the crushing plate were manually removed and fed again.



Figure 11: Circular vibratory screen with two screen decks



Figure 12: Cone crusher in operation

Laboratory comminution tests with primary raw materials

Laboratory comminution tests with a jaw crusher were carried out at Technology Center of RHI Magnesita GmbH in Leoben. For these tests following raw materials for refractory manufacturing were used: sintered magnesia, fused magnesia (see Figure 13) and two different samples of Hercynite (see Figure 14).

To prevent over-comminution, the samples underwent sieving into fractions >20 mm, 10/20 mm, 10/5 mm and <5 mm. Only fractions >20 mm were crushed with the jaw crusher – to ensure similar conditions to industrial trials and obtain comparable results, the gap width was set to 40 mm fixed (see Figure 15). The samples of sintered and fused magnesia were not crushed due to the fact, that these were already classified as <40 mm. Therefore, only the two different samples of Hercynite >20 mm (see Figure 15) had to be crushed and sieved (>20 mm, 10/20 mm, 10/5 mm and <5 mm) once again. As a 40 mm mesh sized screen was not available, the total amount of the fraction >20 mm had to be comminuted. Fractions were weighed and documented for further evaluation of particle size distribution.

Particle shape distributions of particles >10 mm were analyzed in the laboratory (see green highlighted fractions in Figure 16).



Figure 13: Laboratory crushing tests – particle size classes
(left: fused magnesia >20 mm, right: sintered magnesia 0–40 mm)



Figure 14: Laboratory crushing tests – particle size classes (left: Hercynite 1 >20 mm, right: Hercynite 2 >20 mm)



Figure 15: Laboratory crushing tests – jaw crusher

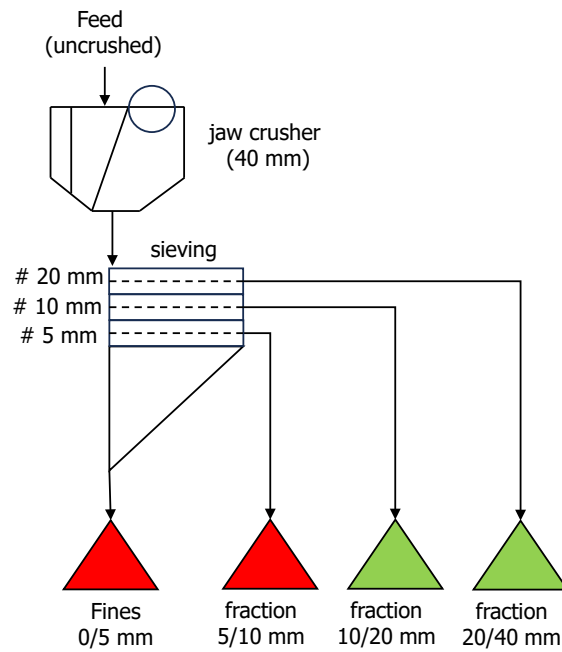


Figure 16: Laboratory crushing tests – flow sheet jaw crusher

3.3 Conventional and alternate comminution, <5 mm

To evaluate the best comminution technology for particle liberation in spent refractory bricks, four technologies were selected for testing to achieve a particle size <5 mm:

1. Jaw crusher: Fractions <4 mm from “Conventional Comminution, <120 mm” trials are used
2. Impact crusher: Fractions <4 mm from “Conventional Comminution, <120 mm” trials are used
3. Cone crusher: Fractions <4 mm from “Conventional Comminution, <120 mm” trials are used
4. EDF lab-scale: Fractions <4 mm will be created with EDF trials on lab-scale at MUL

It was decided to focus on two particle size classes: 4–3.15 mm and 3.15–1 mm. Fully liberated particles typically appear at a particle diameter of <5 mm, which is the maximum particle diameter in refractory raw material. Conversely, particle diameters >4 mm must be conglomerates for this reason.

EDF fractions with particle sizes <4 mm will be created with the selfFrag lab at MUL; therefore a 4 mm sieve will be used in the selfFrag lab process vessel for the trials. At first a parameter study is performed to evaluate, which parameters influence the comminution result of EDF on lab-scale.

Furthermore, it was decided to focus on the materials MgO-C and Hercynite for these trials. At the end the liberation / intergrowth pattern evaluation is done with a combination of

- element analysis
- and density tests (sink-float-analyses).

The chemical composition of the comminution products and fractions was determined using X-Ray Fluorescence analysis (XRF). For carbon-containing bricks, additional carbon analysis was conducted using the combustion method by LECO.

It should be noted that the elemental analysis was performed with a handheld XRF device, which lacks the advanced calibration for refractory materials and higher resolution of laboratory XRF systems. Consequently, handheld devices provide lower accuracy and precision due to their less sophisticated instrumentation and measurement conditions.

3.4 Fractional class analysis

A fractional class analysis is a valuable method to categorize and evaluate a material's distinct properties, such as density, particle size, or susceptibility. By understanding specific material characteristics and determining the degree of particle liberation, this analysis can help to optimize separation and processing techniques and supports continuous process improvement.

The graphic tool used to interpret the results of a fractional class analysis are washability curves plotted in a Henry-Reinhardt (HR) diagram. Which is basically a graphical representation of mineralogical or chemical information and physical parameters of separability. [9] Sinking analysis is a method developed for coal in which ash-containing coal is washed in a liquid with a density between that of the refined coal and the ash. In this case, the clean coal sinks while the ash floats. Therefore, the sink-float test evaluates the compliance of the coal to the gravity concentration method. Selectivity curves are made from the floatation and sinking data and can be used to obtain and interpret valuable information about clean coal or coal quality. [10] Within the scope of this study, selectivity curves will be created for the experimental results of density investigations of MgO-C. They are used to investigate different enrichment ratios of MgO and C at different density classes. The HR diagrams also provide results on the best possible separation within a particle size class based on the prevailing liberation.

Figure 17 shows a simplified version of the HR diagrams with two basic coeval curves (curves A and B). Curve A represents effective separation due to sufficient liberation, whereas curve B represents deficient separation based on the selected property. [11]

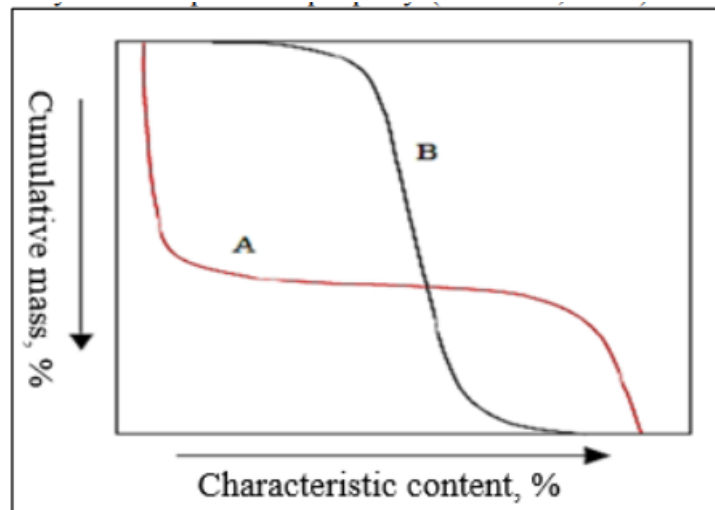


Figure 17: Simplified Henry Reinhardt chart [11]

For the swim-sink-analysis the utilized heavy media was sodium polytungstate, a salt mixed with a certain amount of distilled water to prepare a fluid with the required density (Figure 18). The fluid densities were measured with a hydrometer or with a hydrostatic balance.

Additionally, a suspension of sodium polytungstate and tungsten carbide powder was used to increase the density of the media up to 3.8 g/cm^3 . Tungsten carbide powder does not interfere with subsequent carbide measurements because the powder is dissolved in the liquid phase and is later regenerated from the solution. This assumption is supported by the observation that there is no measurable mass loss of tungsten carbide after the regeneration process. The sample is placed in a beaker glass, filled with the heavy liquid. Particles with a lower specific density than that of the heavy liquid float on the surface, while the remaining particles settle at the bottom.

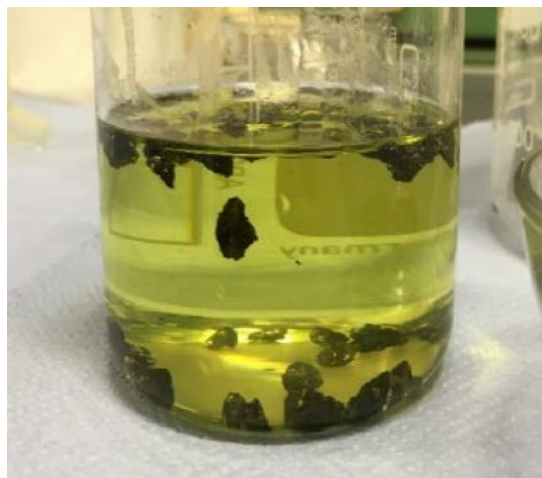


Figure 18: Sodium polytungstate solution for sink-float-analysis, density 3.00 g/cm^3

The experimental design to evaluate particle liberation and intergrowth for the different comminution technologies is visualized in Figure 19.

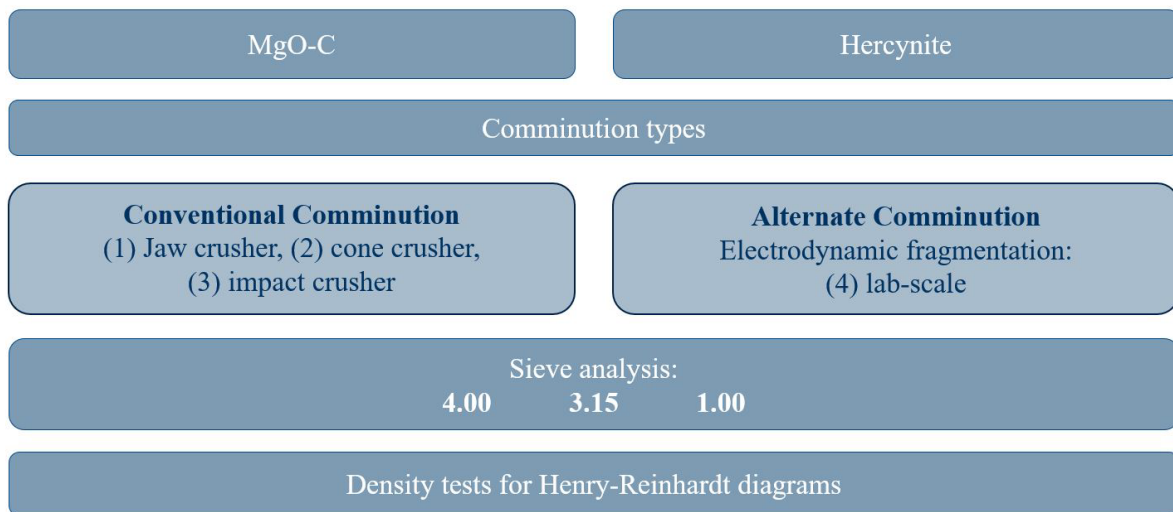


Figure 19: Scheme for the trials to evaluate the particle liberation for the different comminution technologies

Preparation of heavy liquid

The base material to produce the heavy liquid is sodium polytungstate present as white granules, with a molecular mass of 2986.12 g/mol. The density of the prepared solution, showing a transparent to yellow color, can be adjusted. Sodium polytungstate is non-toxic, odorless, neutral and stable. It offers a high recovery rate due to efficient evaporation and crystallization of the residual liquid from rinsing the product after separation.

Density trials

The experimental setup for the density trials is illustrated in Figure 20. The testing procedure is summarized in the following paragraph:

- The sample weight is determined
- The prepared heavy liquid solution is cautiously filled into the beaker and the sample is added to be separated by density.
- Three dispensing funnels are prepared, labelled (light product, heavy product and washing water), and equipped with a 12–15 μm filter paper.
- The floating fraction is transferred to the light product funnel, while the remaining liquid and the settled heavy product are introduced into the heavy product funnel.
- Thus, two products, light product and heavy product, are obtained and the heavy liquid is recovered through the filtration step. Both products are rinsed repeatedly with distilled water until they are entirely free from the solution.
- The cleaned products are dried in a laboratory oven at 70°C.



Figure 20: Experimental setup for the density trials

Element analysis

Follow-up analyses are conducted to determine the chemical composition of the MgO-C and Hercynite fractions. An XRF handheld device is used to detect iron (Fe), aluminum (Al) and magnesium (Mg) and the carbon (C) content is evaluated with LECO. By analyzing the relationship between the sorting density and the products and determining whether element contents increase for specific particle sizes, it is possible to define intergrowth ratios and the degree of particle liberation.

Sample preparation:

3.0 g of each sample are milled to fulfil the sample preparation requirements for XRF and LECO. The samples were placed in the Pulverisette vacuum ball mill and processed with a rotational speed of 650 rpm for two minutes as can be seen in Figure 21.



Figure 21: Pulverisette vacuum ball mill

XRF measurement for Fe, Al and Mg

The Vanta Olympus XRF handheld analyzer identifies elements ranging from Magnesium (Mg) to Uranium (U). Elements lighter than sodium are measured as a sum under the term “Light elements (LE)”. The calibration program “GeoChem-3” is used to detect and indicate the elements. Since there is no specific calibration for refractories available, there can be deviations in the measured values to the real values, especially considering the high oxygen content of the oxidic base materials.

LECO measurement for C content

LECO can determine the carbon and sulfur content of materials through high temperature combustion. High temperature combustion with non-dispersive infrared detection inside LECO's combustion furnaces provide pure oxygen up to 1.350 °C. When a prepared sample is weighed into a combustion boat and placed into the combustion furnace, carbon (C) and sulfur (S) in the specimen are released as carbon dioxide gas and sulfur dioxide gas.

4 Results and Discussion

This chapter is split up into two subchapters for each of the particle size bands, <120 mm and <4 mm.

4.1 Coarse comminution, <120 mm

Analysis of particle size and particle shape distribution were done at MUL. The analysis aimed to evaluate the particle size and shape distribution of various crushed fractions of spent refractories to identify possible interdependencies between refractory type and used crushing equipment. Therefore, representative subsamples of each fraction >10 mm from the pre-selected crushing equipment step were examined. Consequently, after sample division (coning and quartering by using a cross divider, see Figure 23) single particles were measured with a particle shape slide gauge (see Figure 22). All three dimensions of each single particle were documented to quantify a length/width and length/thickness-ratio.



Figure 22: Analysis of particle size and particle shape distribution – particle shape slide gauge



Figure 23: Analysis of particle size and particle shape distribution – Sample A cone crusher, subsample fraction 20/10 mm

Due to increasing efforts with decreasing particle sizes, the particle shape evaluation was only prepared for particles >10 mm, which is shown in Table 1. In Table 1, "-" indicates fractions that could not be analyzed, while "x" denotes fractions that were analyzed. "Not analyzed" signifies that fractions were not analyzed due to their small particle size, even though it was technically possible.

Table 1: Particle shape distribution – sample and analysis overview

material/sample	unit	fraction >40 mm Circular	fraction >40 mm	fraction 20/40 mm	fraction 10/20 mm	fraction 5/10 mm	fraction 0/5 mm
Hercynite - sample A	Impact Crusher I	-	x	x	x	not analyzed	not analyzed
Hercynite - sample A	Impact Crusher II	-	x	x	x	not analyzed	not analyzed
Hercynite - sample A	Cone Crusher I	-	x	x	x	not analyzed	not analyzed
Hercynite - sample A	Cone Crusher II	-	x	x	x	not analyzed	not analyzed
Hercynite - sample A	Jaw Crusher	-	x	x	x	not analyzed	not analyzed
Hercynite - sample B	Impact Crusher II	-	x	x	x	not analyzed	not analyzed
Hercynite - sample B	Cone Crusher I	-	x	x	x	not analyzed	not analyzed
Hercynite - sample B	Cone Crusher II	-	x	x	x	not analyzed	not analyzed
Hercynite - sample B	Jaw Crusher	-	x	x	x	not analyzed	not analyzed
MgO-C - sample C	Impact Crusher II	-	x	x	x	not analyzed	not analyzed
MgO-C - sample C	Cone Crusher I	x	x	x	x	not analyzed	not analyzed
MgO-C - sample C	Cone Crusher II	-	x	x	x	not analyzed	not analyzed
MgO-C - sample C	Jaw Crusher	-	x	x	x	not analyzed	not analyzed
Sintered Magnesia	Jaw Crusher	-	-	-	x	not analyzed	not analyzed
Fused Magnesia	Jaw Crusher	-	-	x	x	not analyzed	not analyzed
Hercynite 1	Jaw Crusher	-	-	x	x	not analyzed	not analyzed
Hercynite 2	Jaw Crusher	-	-	x	x	not analyzed	not analyzed

The evaluation of particle size distributions focuses on the goal of reduction in particle size (based on pre-processed material <120 mm) while minimizing the fines (<5 mm). Therefore, the mass of the fraction <5 mm as well as the k20 and k80 values were evaluated. The k20 value defines the particle size at passing rate of 20 % while k80 value defines the particle size at passing rate of 80 %. The values are calculated by linear interpolation of nearest by classification defined particle sizes and related mass portions (see Table 2).

Table 2: Comminution characteristics for different crushing equipment and various used refractories

k20 value	Hercynite - sample A	Hercynite - sample B	MgO-C - sample C
Jaw Crusher (gap width 40 mm)	10.96 mm	6.23 mm	6.08 mm
Cone Crusher II (gap width 46 mm)	12.58 mm	10.11 mm	13.94 mm
Impact Crusher II (gap width 40 mm)	1.95 mm	1.83 mm	1.69 mm
k80 value	Hercynite - sample A	Hercynite - sample B	MgO-C - sample C
Jaw Crusher (gap width 40 mm)	36.36 mm	34.54 mm	36.46 mm
Cone Crusher II (gap width 46 mm)	37.30 mm	37.19 mm	37.00 mm
Impact Crusher II (gap width 40 mm)	28.33 mm	21.42 mm	15.45 mm
mass fraction <5 mm	Hercynite - sample A	Hercynite - sample B	MgO-C - sample C
Jaw Crusher (gap width 40 mm)	13.02 %	17.51 %	11.25 %
Cone Crusher II (gap width 46 mm)	11.58 %	11.85 %	11.72 %
Impact Crusher II (gap width 40 mm)	51.40 %	54.50 %	59.03 %

Using the impact crusher showed the highest increase in dispersion expressed by lowest k20 and k80 values in combination with highest mass portions of fraction <5 mm for each examined sample. Within the various spent refractories, sample C (MgO-C) tends to comminute finer than samples A and B (Hercynite). The lowest mass portion of fraction <5 mm with 11.25 % was documented for sample C using the jaw crusher – despite corresponding a high k80 value of 36.46 mm, the k20 value is the lowest among the three samples regarding jaw crusher usage. The lowest values of the fraction <5 mm (in total less than 13.94 %) and preferably high values for k20 (up to 10.96 mm) and k80 (up to 36.46 mm) where demonstrated by using the cone crusher (cone crusher, with settings II).

For Hercynite sample B comminutes finer than sample A – this is valid for all different examined crushing equipment (see Figure 24, Figure 25 and Figure 26).

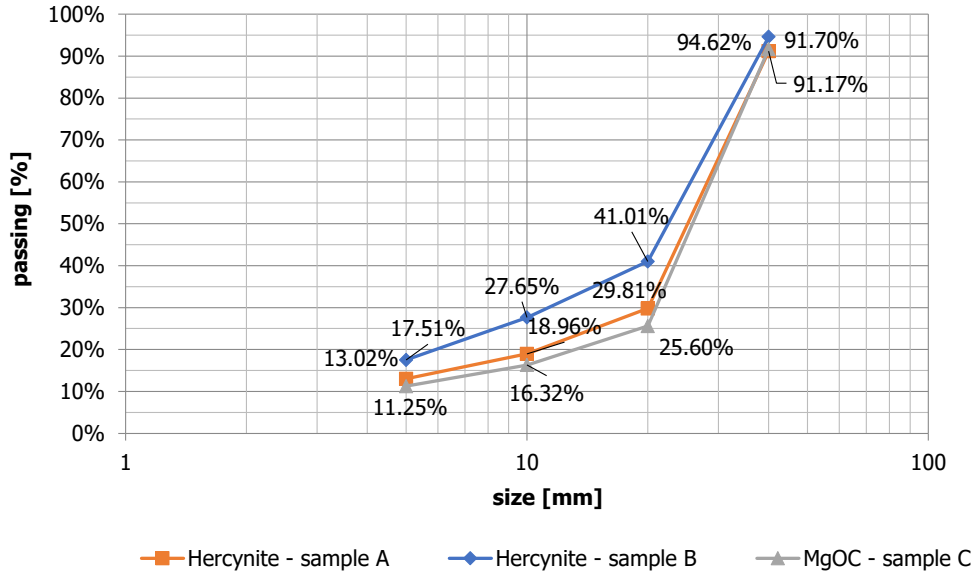


Figure 24: Particle size distribution of various used refractories by using jaw crusher

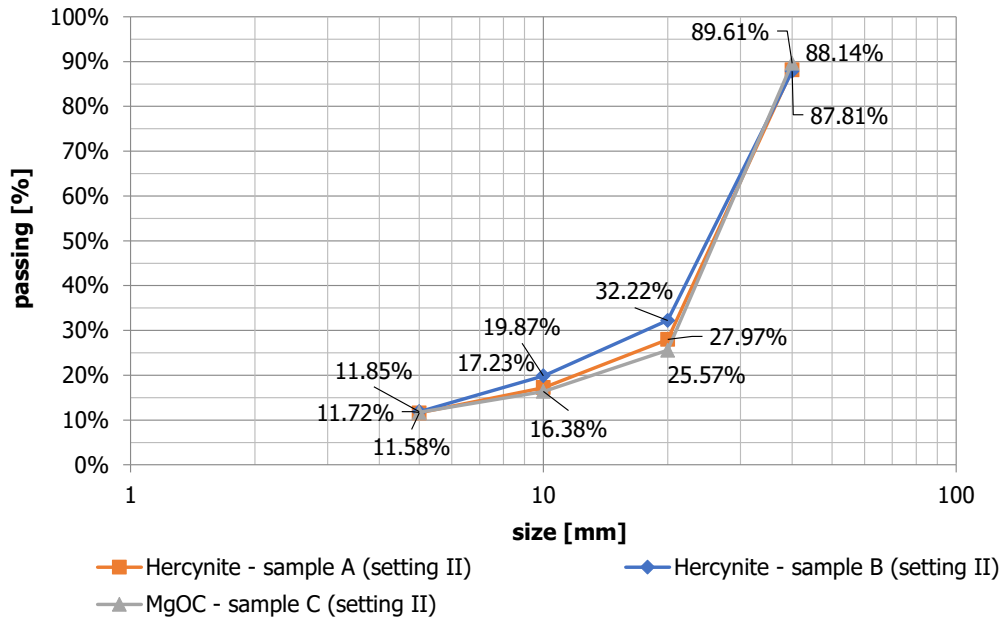


Figure 25: Particle size distribution of various used refractories by using cone crusher

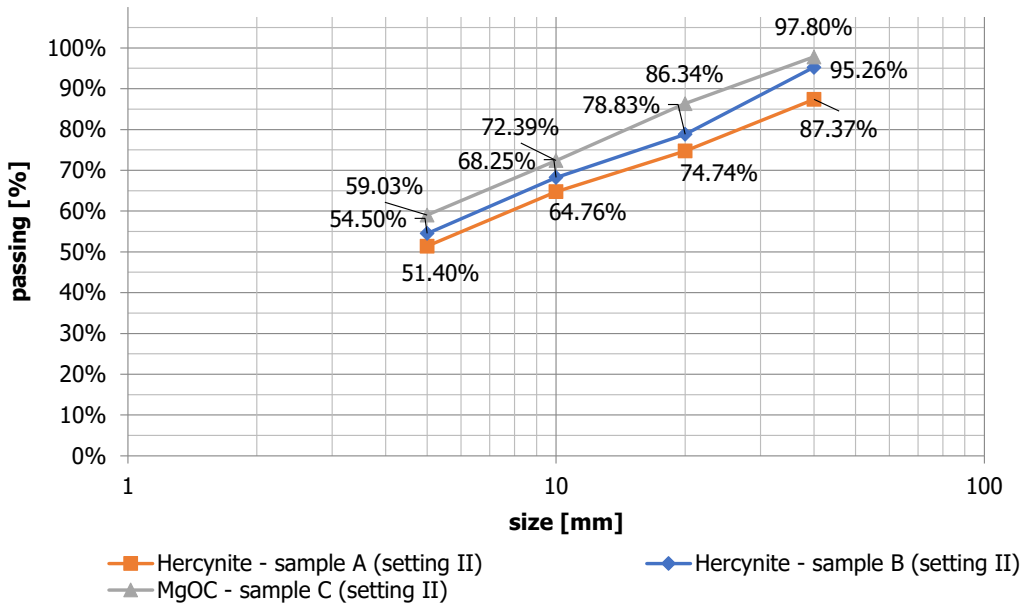


Figure 26: Particle size distribution of various used refractories by using impact crusher

Regarding particle shape characteristics related to different crushing types (more specifically different kinds of stress loading), the cone crusher tendentially led to conchoidal shape of crushed products (expressed by higher length/thickness and length/width ratio). This effect could be observed for all three samples within all different fraction classes. The difference in length/thickness and length/width ratio is smaller between jaw and cone crusher than between impact and jaw crusher. Therefore, the impact crusher results in a more cubic/compact shape. Sample C tends to comminute in a more cubic shape than the other samples (see Figure 30 with lower length/thickness and length/width ratios for MgO-C than for Hercynite).

Hypothesis: The influence of crushing equipment on particle shape is higher than the specific material characteristic of examined refractories.

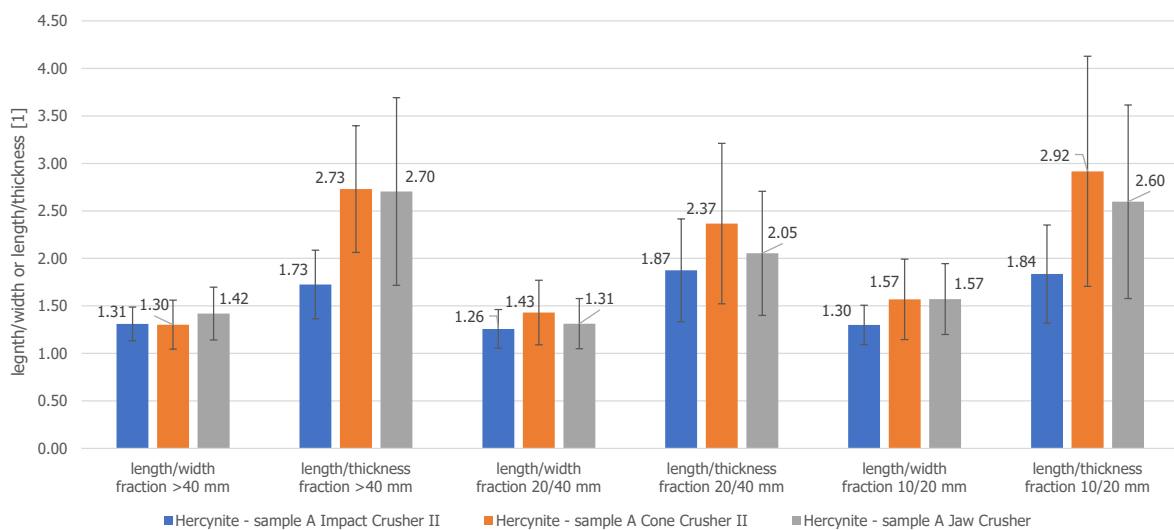


Figure 27: Particle shape distribution sample A (Hercynite A) using different crushing equipment

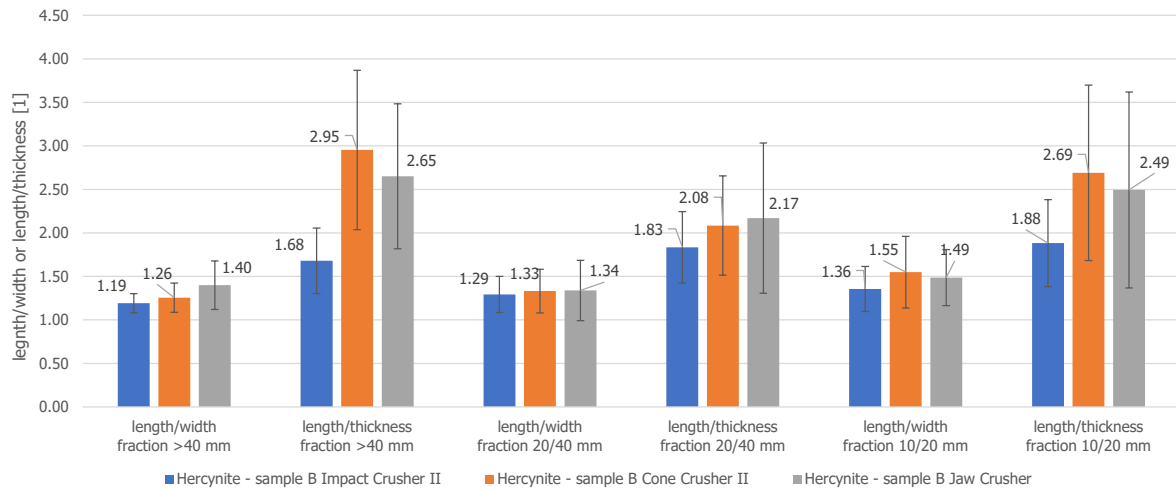


Figure 28: Particle shape distribution sample B (Hercynite B) using different crushing equipment

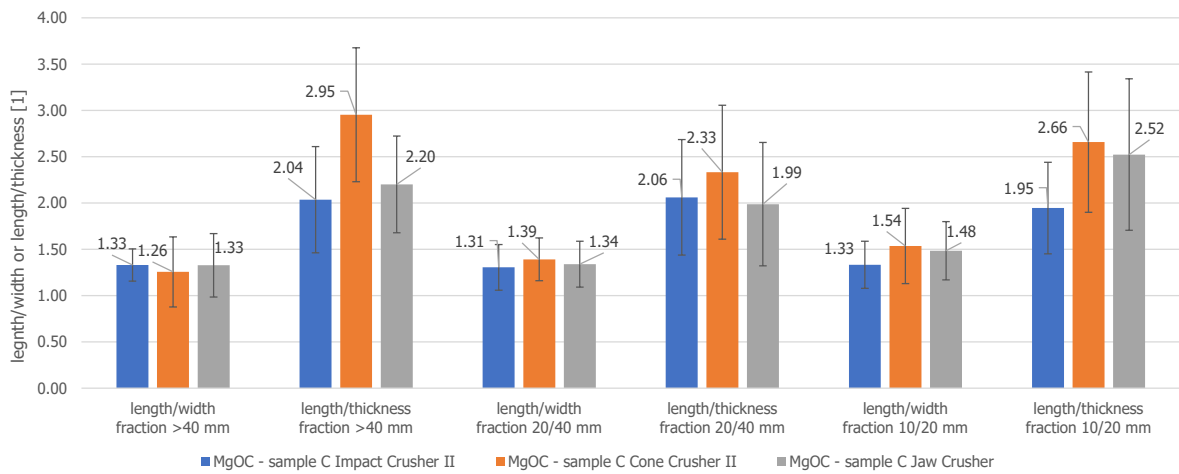


Figure 29: Particle shape distribution sample C (MgO-C) using different crushing equipment

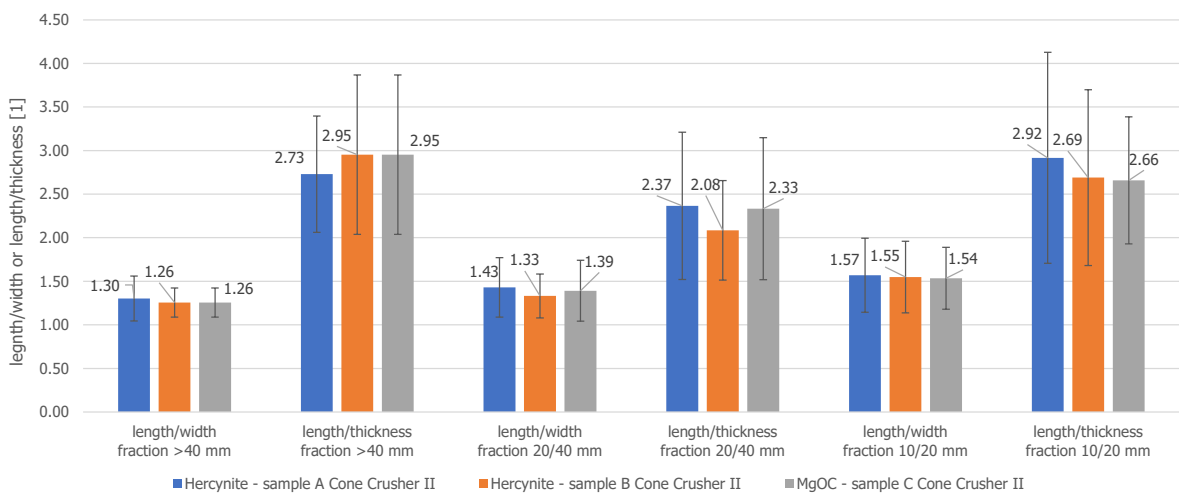


Figure 30: Particle shape distribution for various types of used refractories – cone crusher (setting II)

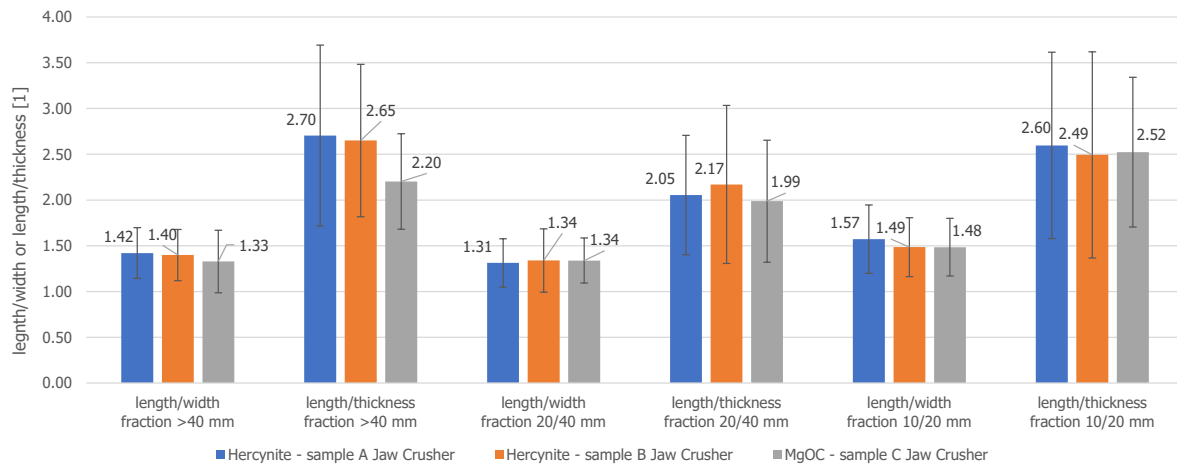


Figure 31: Particle shape distribution for various types of used refractories – jaw crusher

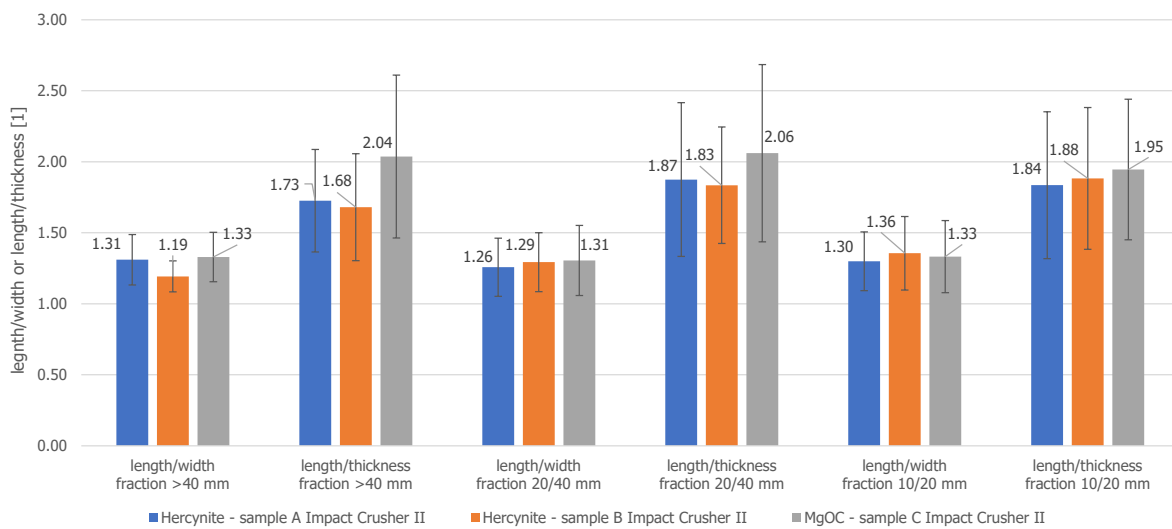


Figure 32: Particle shape distribution for various types of used refractories – impact crusher (setting II)

Chemical analysis of the examined spent refractory samples was provided by RHIM using a refractory calibrated quantitative XRF (see Table 4) and show the complexity of recycling efforts.

Chemical analysis of sample C (MgO-C) shows an interdependence of chemical contents and particle size distribution: The highest amount of total carbon (16.10 %) was documented in particle size class 0–0.5 mm – this content is also reflected in the loss on ignition.

Table 3: Chemical analysis of various used refractories (samples A, B and C)

compounds		sample A (Hercynite)	sample B (Hercynite)	sample C (MgO-C) 5–40 mm				
		0–5 mm	0–5 mm	0–0.5 mm	0.5–1.0 mm	1.0–3.15 mm	3.15–4.0 mm	4.0–6.3 mm
MgO	[%]	79.93	47.34	93.15	94.79	94.52	94.47	94.42
Al ₂ O ₃	[%]	10.10	24.45	3.01	1.92	1.86	1.88	1.52
SiO ₂	[%]	1.00	19.72	1.19	0.97	1.10	1.06	1.32
CaO	[%]	2.22	1.39	1.80	1.56	1.67	1.66	1.80
Fe ₂ O ₃	[%]	4.30	4.93	0.71	0.63	0.70	0.77	0.74
loss on ignition	[%]	3.35	3.08	18.30	11.90	12.20	9.51	15.2
C-total	[%]	not measurable	not measurable	16.10	10.40	10.70	8.16	8.95
S	[%]	not measurable	not measurable	0.063	0.042	0.046	0.043	0.054

4.2 Conventional and alternate comminution, <4 mm

Electrodynamic fragmentation on lab-scale as alternate comminution technology

To characterize the behavior of refractories in a lab-scale EDF setup, all samples were sieved and categorized into the following classes: 5–10 mm, 10–20 mm, 20–40 mm and 5–40 mm. After sieving, the self-fragmentation test was conducted with a sample from each class applying different sets of parameters which are listed in Table 4 below.

Table 4: Codification of samples in the experiment

Codification	Volt [kV]	Pulse [-]
Sample I	150	60
Sample II	150	100
Sample III	200	60
Sample IV	200	100

Voltage and pulse parameters are adjusted to modulate energy levels and analyze comminution behavior, with minimum thresholds of 150 kV and 60 pulses. Frequency, electrode gap, and screen size remain fixed at 50 Hz, 40 mm, and 4 mm respectively, due to operational constraints and equipment specifications of the pilot plant. After self-fragmentation test, the product of each feed and each set of parameters was dried at 70°C for 24 hours and then sieved to analyze the particle size distribution. In addition, the process water was collected to measure the pH and conductivity.

MgO-C Comminution using EDF

The result of the processing of MgO-C shows a significant size reduction compared to the feed size. The comparison of the particle size distribution between the product and feed is illustrated in Figure 33 and Figure 34. Samples 4 (for 10–20 mm sample band) and 2 (for 5–40 mm sample band) yield the finest products for trials with set parameters at 200 kV and 100 pulses. The resulting k80 product values are 2346 μm and 11974 μm respectively.

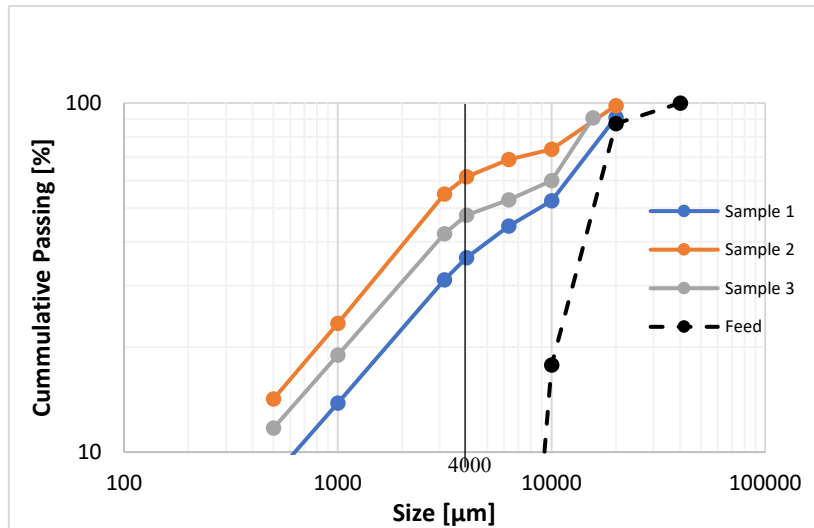


Figure 33: Product & feed particle size distribution of MgO-C 5–40 mm sample band

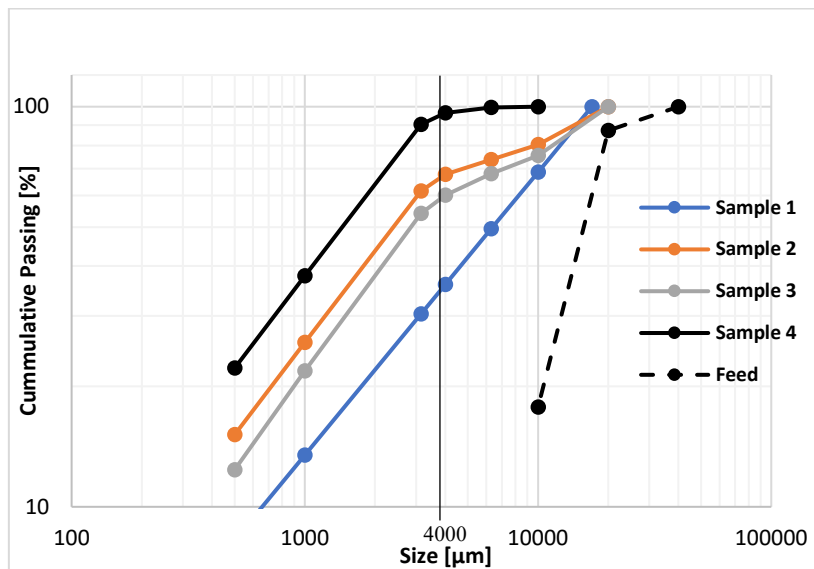


Figure 34: Product & feed particle size distribution of MgO-C 10–20 mm sample band

Effect of Pulses and Voltage on MgO-C Comminution

Figure 35 and Figure 36 show that voltage variation reduces the product size (k80 product), while number of pulses is kept constant at 60. The same behavior occurs when the pulse is varied from 60 to 100, while keeping the voltage constant at 150 kV in Figure 37 and Figure 38. However, the k80 product generated from the parameter 150 kV and 100 pulses is lower than k80 product generated from the parameter 200 kV and 60 pulses. The results imply that in a 60 pulses process, changing the voltage will not contribute significantly to reduce the particle size, even though the generator emits more energy to the medium (water).

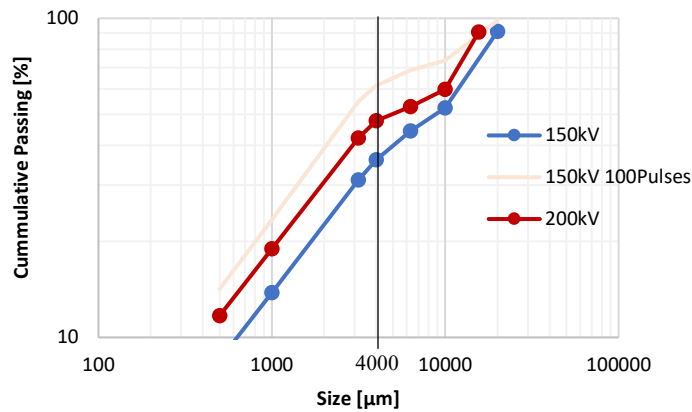


Figure 35: Effect of Voltage on Particle Size Distribution of MgO-C Product from Feed Size 5–40 mm (Constant Pulse: 60)

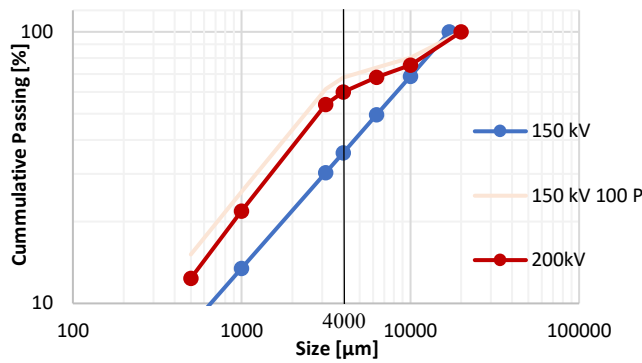


Figure 36: Effect of Voltage on Particle Size Distribution of MgO-C Product from Feed Size 10–20 mm (Constant Pulse: 60)

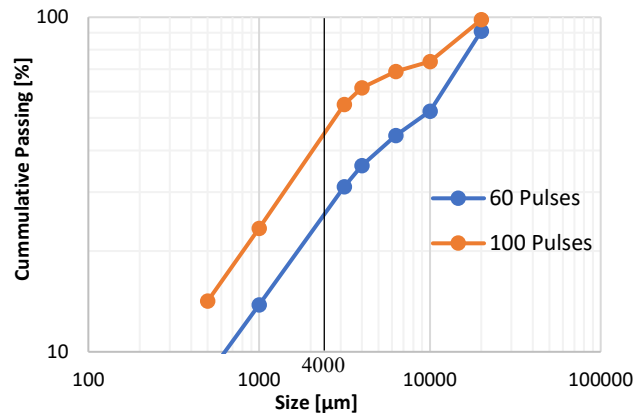


Figure 37: Effect of Pulses on Particle Size Distribution of MgO-C Product from Feed Size 5–40 mm (Constant V: 150 kV)

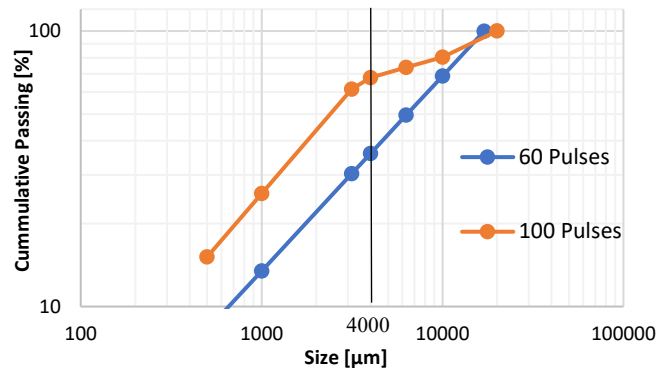


Figure 38: Effect of pulses on Particle Size Distribution of MgO-C Product from Feed Size 10–20 mm (Constant V: 150 kV)

The reason for the observed behavior can be explained by observing the amount of energy penetrating the material (spark energy). Table 5 displays that the spark energy generated from 200 kV and 60 pulses parameter set is lower than the spark energy from 150 kV and 100 pulses parameter set, even though generator energy emitted for 200 kV and 60 pulses is higher. It can be concluded that it is favorable to operate the machine at 100 pulses rather than 60 pulses when the voltage is set to 150 kV, due to higher energy efficiency.

Table 5: Parameters of EDF setting correspond to energy generator, spark energy and efficiency

Material	Particle Size Class [mm]	Pulse [-]	Voltage [kV]	E generator [kWh/t]	E spark [kWh/t]	Efficiency [%]
MgO-C	5–40	60	150	14.00	8.69	62
MgO-C	5–40	100	150	23.38	15.46	66
MgO-C	5–40	60	200	24.95	12.87	51
MgO-C	10–20	60	150	14.06	10.50	75
MgO-C	10–20	100	150	23.44	18.78	80
MgO-C	10–20	60	200	25.00	16.44	66

On the other hand, Figure 39 shows that with 100 pulses set as constant, different levels of voltage start to show significant differences. The size of the k80 of product generated from 200 kV - 100 pulses is lower than 150 kV and 100 pulses.

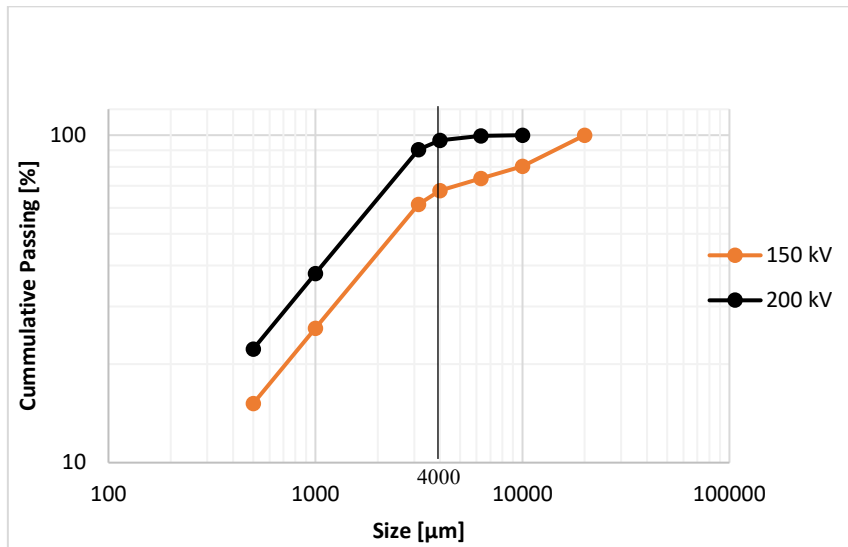


Figure 39: Effect of voltage variation on the size distribution of the MgO-C product while operating on constant 100 pulses

Considering the energy table (Table 6), there is a correlation between energy absorbed by the material and the significant size reduction because of the comminution. The parameter set of 200 kV - 100 pulses create 60 % more spark energy, energy that penetrates the feed material, than the 150 kV - 100 pulses parameter set. It explains why the k80 product of 200 kV - 100 pulses is low even though the energy efficiency is lower than the 150 kV - 100 energy efficiency. Besides lower size of k80 product, the 200 kV - 100 pulses experiment also generates a larger fraction below 4 mm.

Table 6: Parameters of EDF setting correspond energy and its efficiency from 150 kV – 100 P and 200 kV – 100 P

Materials	Particle Size Class [mm]	Pulses [-]	Voltage [kV]	E generator [kWh/ton]	E spark [kWh/t]	Efficiency [%]
MgO-C	10–20	100	150	23.44	18.78	80
MgO-C	10–20	100	200	41.67	30.39	73

Hercynite comminution using EDF

Figure 40 demonstrates that an increase in voltage and pulses result in finer comminution and an accompanying rise in cumulative passing for Hercynite samples 1 to 4 (fraction 5–10 mm).

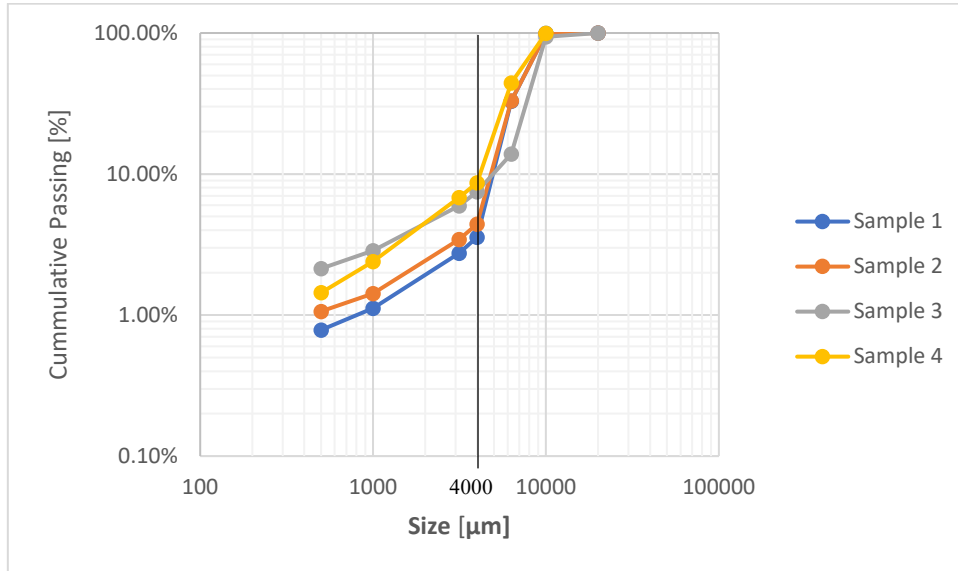


Figure 40: Particle size distributions of four samples of Hercynite product of feed size 5–10 mm

Figure 41 displays the same behavior for the fraction 20–40 mm of the same samples.

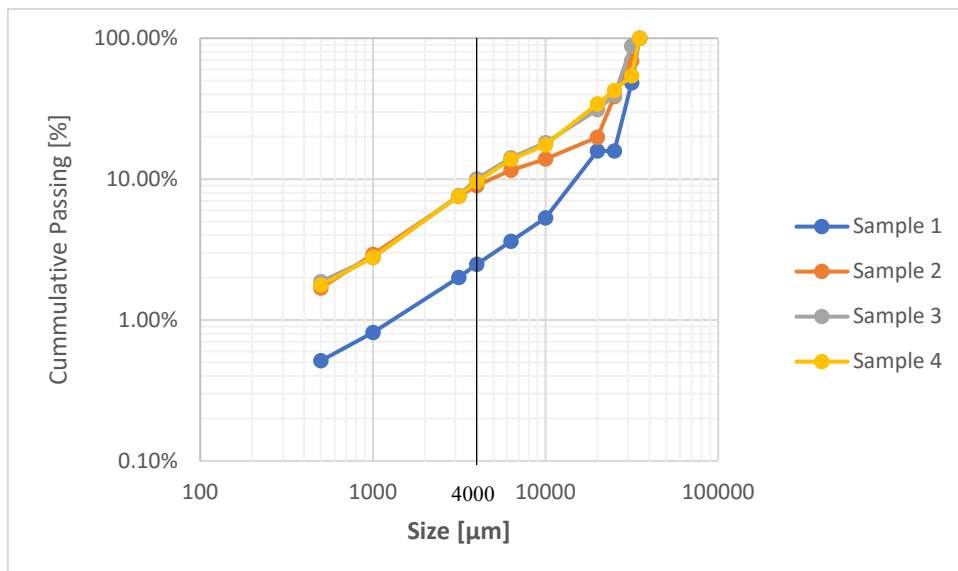


Figure 41: Particle size distribution of four samples of Hercynite product of feed size 20 - 40 mm

The comparison (Figure 42) of the particle size distributions of Hercynite samples with feed size 5–10 mm and 20–40 mm shows that the Hercynite samples 20–40 mm have larger fractions below 4 mm compared to 5–10 mm samples at 200 kV and 100 pulses.

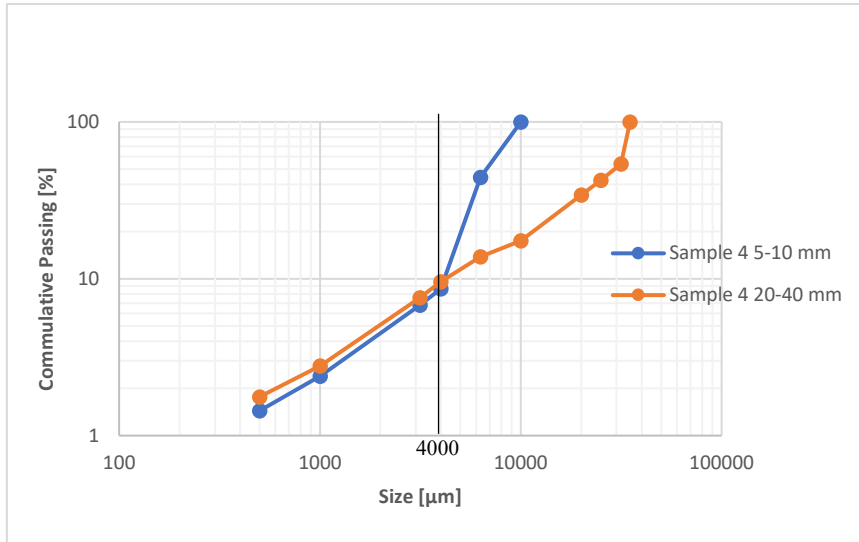


Figure 42: Comparison of Hercynite Particle Size Distributions from feed size 5–10 and 20–40 mm at 200 kV and 100 pulses

Effect of EDF comminution to the process water obtained from the process vessel

The EDF comminution process of MgO-C and Hercynite changes the properties of the used processing water by contaminating the water during the process. Figure 43 displays that the water conductivity is increased after the EDF process. Samples belonging to the sorting class Hercynite are infiltrated with alkaline salts, being solved in the water during the process (see section 3.1) and increasing the conductivity of the process water more significantly than samples belonging to the sorting class MgO-C. The conductivity of the process water reached levels of up to 1200 $\mu\text{S}/\text{cm}$. In case of Hercynite, the EDF was less effective compared to MgO-C, shown in Figure 43. One reason might be the increased water conductivity due to the contaminations, which leads to a loss of pulse energy, resulting in weak comminution. Another reason could be insufficient differences in the raw material properties.

Besides altering the conductivity, the comminution process also affects the pH value of the water. For MgO-C and Hercynite, the change in pH of the water ranges from 6 to 9.2–9.7, due to the basic character of the samples (Figure 44). For a potential upscaling of EDF, a wastewater treatment might be considered.

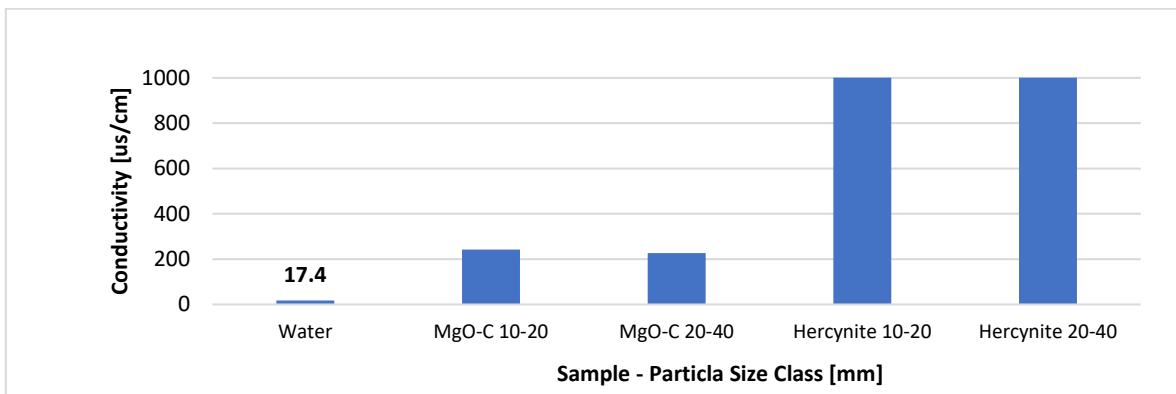


Figure 43: Effect of MgO-C and Hercynite EDF comminution to the conductivity of the process water after 100 pulses

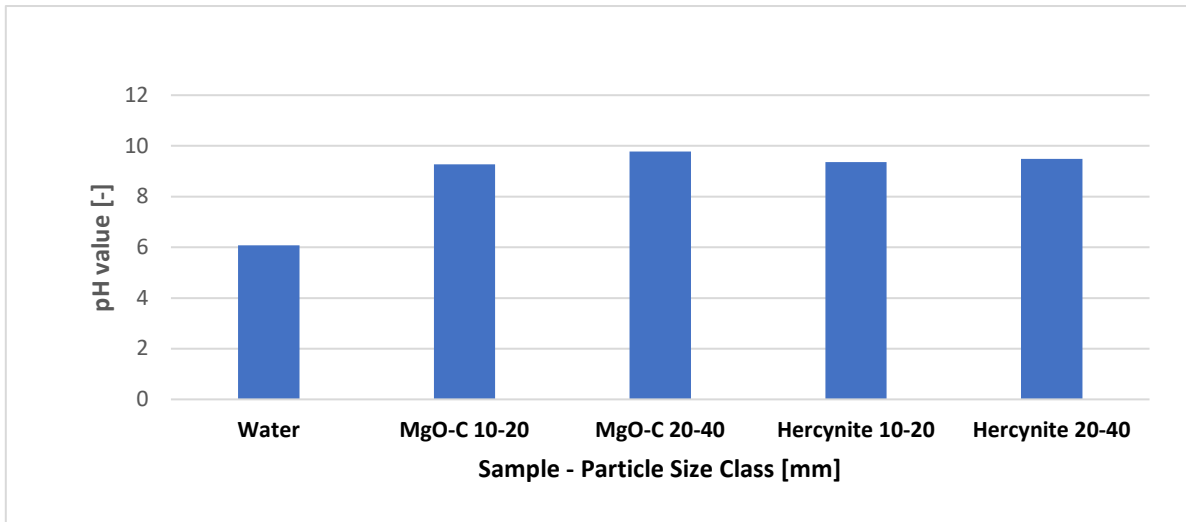


Figure 44: Effect of MgO-C and Hercynite EDF comminution to the pH value of the process water after 100 pulses

4.3 Fractional class analysis

MgO-C fractional class analysis

Referring to D1.2 the main components of MgO-C refractory bricks with their density ranges can be seen in Table 7. It shows that the two main components are MgO and C, so a density separation can be evaluated with an element measurement of Mg and C. (No oxygen is bound in C).

Table 7: Main components of MgO-C refractory bricks with their densities

MgO-C	Component	Density [g/cm ³]
Periclase	MgO	3,58
Graphite	C	2,26

Density tests: Pre-trials to find suitable separation densities

The selected sample for the pre-trials to find suitable separation densities is “MgO-C Jaw crusher 4–3.15 mm”. Determined separation densities are given in Table 8, together with the shares of light and heavy products, respectively.

Table 8: Data of pre-trials for the determination of suitable separation densities

Separation density [g/cm ³]	Light product [%]	Heavy product [%]
2.7	1.57	>98
3.0	20.44	>70
3.5	56.98	19.38

The results of the pre-trials can be seen in Figure 45. The experiment resulted in three distinct separable densities 2.7 g/cm³, 3.0 g/cm³ and 3.5 g/cm³, creating four density classes: <2.7 g/cm³, 2.7–3.0 g/cm³, 3.0–3.5 g/cm³, >3.5 g/cm³. The product mass in the fraction below 2.7 g/cm³ is negligibly small. A clear visual difference can be observed between the products in the <3.0 g/cm³ and >3.0 g/cm³ density classes. These findings provide justification for using 3.0 g/cm³ as a separation density to distinguish MgO-rich from C-rich fractions at first.

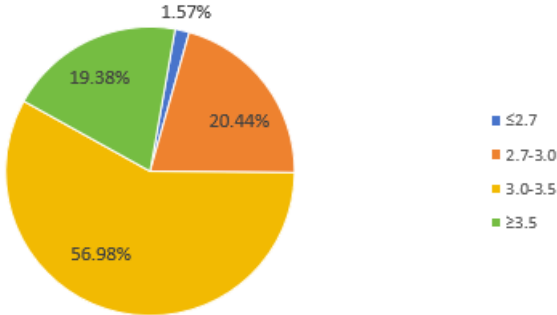


Figure 45: Results of the pre-trials to find suitable separation densities

MgO-C density trials

Through fractional class analysis based on differences in density, the experiment ultimately led to products in four different density classes for each particle size class: <2.7 g/cm³, 2.7–3.0 g/cm³, 3.0–3.5 g/cm³ and >3.5 g/cm³. In the following section Henry-Reinhardt (HR) diagrams are used to visualize the results of the density separation trial exemplarily for the fraction 4–3.15 mm originating from the jaw crusher comminution experiments. The HR-diagram shows that the grades of Mg are 56 % and 58 % for >3.5 g/cm³ and 3.0–3.5 g/cm³, respectively, proving that Mg is enriched when the density is >3.0 g/cm³. Since the only two components of MgO-C are MgO and C, it is assumed that the Mg content represents the MgO content.

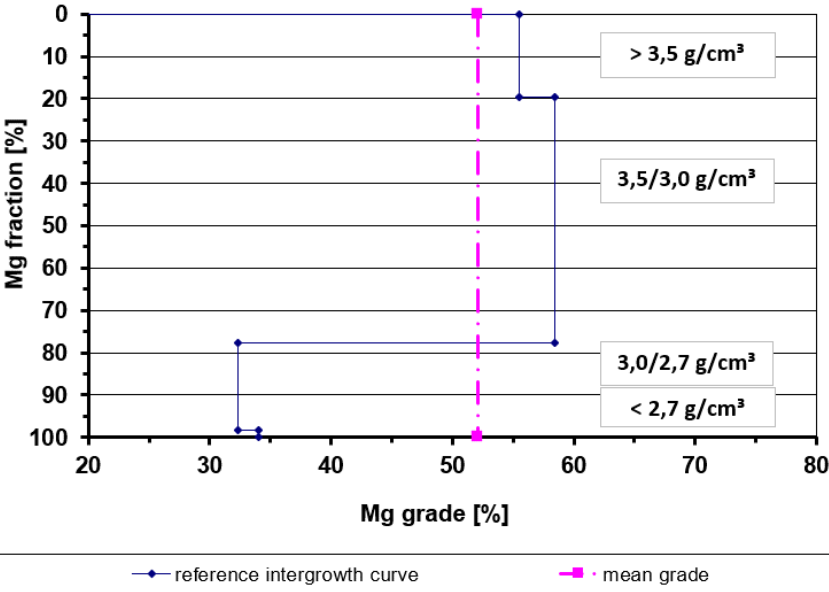


Figure 46: HR-diagram for MgO-C Jaw crusher 4–3.15 mm of Mg grade

However, the diagram in Figure 46 shows the enrichment ratios for Mg between $<2.7 \text{ g/cm}^3$ and $2.7\text{--}3.0 \text{ g/cm}^3$ are very similar, 34 % and 32 % respectively. Conversely, the HR diagram for carbon (Figure 47) demonstrates an increased carbon content in the products $<3.0 \text{ g/cm}^3$.

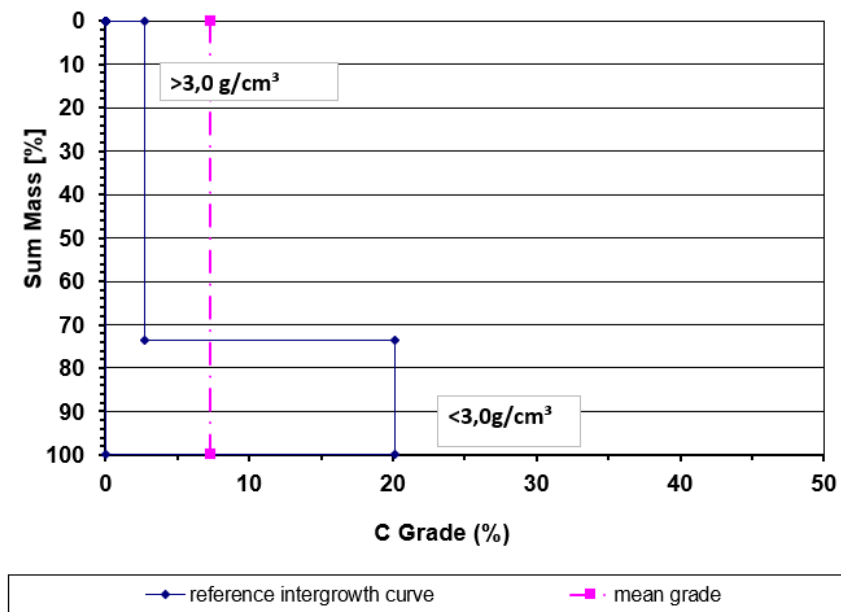


Figure 47: HR diagram for MgO-C comminuted with a jaw crusher and a particle size 4–3.15 for carbon grade

Assessing the results, it needs to be considered that the element analysis is done with a XRF handheld, which does not have a as high measurement accuracy as XRF lab measurements. The results for the MgO-C density trials with a heavy liquid of 3.0 g/cm^3 are visualized in Table 9 and can be summarized as follows:

1. The results reveal that regardless of the particle size class, C can be enriched in the density class $<3.0 \text{ g/cm}^3$ and Mg in the density class $>3.0 \text{ g/cm}^3$ (Table 9 in green) except for lab-scale EDF and cone crusher, where no significant Mg enrichment was achieved in the particle size class 3.15–1 mm (Table 9 in red). EDF as a comminution technology leads to the least favorable result in Mg-enrichment compared to conventional comminution technologies for a density of $>3.0 \text{ g/cm}^3$ with 45.5 % (4–3.15 mm,) and 38.5 % (3.15–1 mm). The cone crusher shows that an Mg enrichment was unsatisfactory for a density of $>3.0 \text{ g/cm}^3$ with 21.5 % (3.15–1 mm).
2. The carbon enrichment in the density class $<3.0 \text{ g/cm}^3$ yielded positive results for all comminution technologies with contents ranging between 17.6 and 21.6 %.
3. The jaw crusher shows the highest performance in liberating particles, resulting in the maximum enrichment of C and Mg achieved in two density classes.

Interpreting the key message of the HR diagram, it can be concluded that for the given material a density separation cut at 3.0 g/cm^3 yields a mass recovery of approximately 80% for an Mg-rich concentrate, with an average Mg grade of around 58%.

Sums in Table 9 are calculated for “m total”, “m fraction” and the mass sum of specific elements in the whole sample to get a better understanding for the success of the enrichment in specific fractions. Further, the table displays the amounts of Mg and C as relevant elements for MgO-C. The amounts of further elements can be found in the Appendix. Last, it needs to be mentioned, that C was measured with LECO and Mg with XRF. For this reason, these amounts cannot be summed up.

Table 9: Results for the MgO-C density trials with a heavy liquid of 3.0 g/cm³

Refractory	Comminution technology	Particle size [mm]	m total [g]	fraction [%]	m sample [g]	m loss [g]	fraction loss [%]	density [g/cm ³]	m sample [g]	C (LECO) [%]	C sample [g]	C total [g]	Mg (XRF) [%]	Mg sample [g]	Mg total [g]	LE (XRF) [%]	
MgO-C	Conventional, Jaw crusher	4-3.15	44.8	9.4	32.5	0.3	1.0	<3.0	6.8	20.2	1.4	2.8	32.3	2.2	23.7	41.9	
								>3.0	25.4	2.7	0.7		58.5	14.8		36.1	
		3.15-1	205.8	43.2	42.5	0.4	1.1	<3.0	11.5	21.3	2.5	19.9	32.7	3.8	79.4	39.9	
								>3.0	30.5	5.3	1.6		40.8	12.5		52.9	
		<1	225.8	47.4	5.0	-	-	-	5.0	15.8	0.8	35.7	44.7	2.2	100.9	47.2	
		Sum	476.3	100.0	-	-	-	-	-	-	-	58.4	-	-	-	204.0	-
		Conventional, Impact crusher	4-3.15	33.5	11.8	22.5	0.1	0.7	<3.0	6.4	17.6	1.1	2.5	40.7	2.6	15.9	33.8
									>3.0	16.0	3.5	0.6		49.9	8.0		39.8
	3.15-1		122.3	43.2	110.0	0.2	0.2	<3.0	27.4	21.0	5.8	10.3	30.4	8.3	43.2	50.6	
								>3.0	82.4	4.2	3.5		37.0	30.5		37.7	
	<1		127.2	44.9	5.0	-	-	-	5.0	18.2	0.9	23.2	43.2	2.2	55.0	47.3	
	Sum		283.1	100.0	-	-	-	-	-	-	-	35.9	-	-	-	114.0	-
	Conventional, Cone crusher		4-3.15	39.6	13.4	18.0	0.3	1.5	<3.0	4.2	18.9	0.8	2.7	41.2	1.7	19.2	30.9
									>3.0	13.5	3.2	0.4		51.0	6.9		39.5
		3.15-1	133.7	45.4	115.0	1.4	1.3	<3.0	86.2	21.6	18.6	22.8	44.1	38.0	55.9	50.2	
								>3.0	27.3	2.8	0.8		34.8	9.5		24.7	
		<1	121.5	41.2	5.0	-	-	-	5.0	17.8	0.9	21.6	46.8	2.3	56.8	42.2	
		Sum	294.8	100.0	-	-	-	-	-	-	-	47.2	-	-	-	132.0	-
		EDF Lab, 5-10 mm, sample IV	4-3.15	31.6	6.3	25.5	0.5	2.0	<3.0	9.3	18.9	1.8	2.7	39.3	3.6	13.6	30.7
									>3.0	15.7	2.4	0.4		45.5	7.1		43.5
	3.15-1		265.1	53.1	75.0	0.6	0.8	<3.0	30.0	20.9	6.3	30.4	30.0	9.0	66.1	30.1	
								>3.0	44.4	5.1	2.3		21.5	9.6		38.7	
	<1		202.8	40.6	5.0	-	-	-	5.0	16.9	0.8	34.3	38.5	1.9	78.1	40.3	
	Sum		499.5	100.0	-	-	-	-	-	-	-	67.4	-	-	-	157.8	-

m total [g] Mass of the particle size class from the fine fraction samples PSD
fraction [%] Mass percentage of the particle size class from the fine fraction samples PSD
m sample [g] Mass of the sample, which was used for the density tests
m loss [g] Mass of sample loss during the density trial
fraction loss [%] Mass percentage of sample loss during the density trial
Density [g/cm³] Density class in which fraction enriched after the separation process
Element (xx) [%] Mass percentage of element in the separated sample, measurement method mentioned in brackets
Element total [g] Mass of the element, which is stored in the particle size class

Hercynite fractional class analysis

Referring to D1.2, the main components of Hercynite refractory bricks with their density ranges are listed in Table 10.

Table 10: Main components of Hercynite refractory bricks with their densities

Hercynite low Fe	Component	Density [g/cm ³]
Hercynite-Spinel	FeAl ₂ O ₄	3.95
Magnesia-Alumina-Spinel	MgAl ₂ O ₄	3.58

Considering the densities of FeAl₂O₄ and MgAl₂O₄ as stated above, the selected density classes are <3.63 g/cm³ and >3.63 g/cm³. As a result, a Hercynite-Spinel enriched fraction and MgAl spinel fraction are the expected products of the separation experiment. The results for the Hercynite density trials with a heavy liquid of 3.63 g/cm³ are visualized in Table 11. They can be summarized with the following statements:

1. According to the low contents and small corresponding masses in the density classes of Fe and Al it is not feasible to create HR diagrams. Due to the lack of gained information from this separation trials, no evaluation of the liberation performance of the different comminution technologies can be carried out.
2. It can be stated that a separation density of 3.63 g/cm³ results in an enrichment of iron despite the low material input (<0.1 g to 9.3 g).

Sums in Table 11 are calculated for “m total”, “m fraction” and the mass sum of specific elements in the whole sample to get a better understanding for the success of the enrichment in specific fractions.

Further, the table displays the amounts of Fe, Al and Mg as relevant elements for Hercynite. The amounts of further elements can be found in the Appendix.

Table 11: Results for the Hercynite density trials with a heavy liquid of 3.63 g/cm³

Refractory	Comminution technology	Particle size [mm]	m total [g]	fraction [%]	m sample [g]	m loss [g]	fraction loss [%]	density [g/cm ³]	m sample [g]	Fe (XRF) [%]	Fe sample [g]	Fe total [g]	Al (XRF) [%]	Al sample [g]	Al total [g]	Mg (XRF) [%]	Mg sample [g]	Mg total [g]
Hercynite high Fe (B)	Conventional, Jaw crusher	4-3.15	25.0	12.5	22.0	0.2	0.8	<3.63	21.5	0.6	0.1	0.2	2.8	0.6	0.7	30.5	6.6	7.6
								>3.63	0.3	8.6	0.0		7.0	0.0		16.2	0.1	
		3.15-1	142.8	71.3	61.0	0.6	0.9	<3.63	51.2	0.4	0.2	0.7	0.6	0.3	1.0	38.0	19.4	57.1
								>3.63	9.3	0.6	0.1		0.9	0.1		51.3	4.8	
		<1	32.5	16.2	5.0	-	-	-	5.0	2.9	0.1	0.9	9.7	0.5	3.2	18.1	0.9	5.9
		Sum	200.3	100.0	-	-	-	-	-	-	-	1.8	-	-	4.8	-	31.7	70.6
	Conventional, Impact crusher	4-3.15	28.1	9.9	15.0	0.3	1.9	<3.63	14.3	1.6	0.2	0.4	8.8	1.3	2.4	29.8	4.3	8.4
								>3.63	0.4	0.7	0.0		4.5	0.0		30.6	0.1	
		3.15-1	159.6	56.4	45.0	0.5	1.1	<3.63	40.5	1.5	0.6	4.2	15.2	6.2	24.0	18.8	7.6	29.7
								>3.63	4.0	13.8	0.6		12.9	0.5		17.3	0.7	
		<1	95.4	33.7	5.0	-	-	-	5.0	3.3	0.2	3.1	8.5	0.4	8.1	16.3	0.8	15.5
		Sum	283.1	100.0	-	-	-	-	-	-	-	7.7	-	-	34.5	-	13.5	536
Conventional, Cone crusher	4-3.15	67.1	14.7	22.5	0.2	1.1	<3.63	22.1	1.2	0.3	0.8	3.4	0.7	2.3	46.7	10.3	31.2	
							>3.63	0.2	0.5	0.0		9.8	0.0		19.3	0.0		
	3.15-1	246.6	53.9	43.0	0.8	1.9	<3.63	37.2	1.1	0.4	2.7	4.8	1.8	11.7	45.7	17.0	112.4	
							>3.63	5.0	1.2	0.1		4.5	0.2		45.0	2.3		
	<1	144.0	31.5	5.0	-	-	-	5.0	2.8	0.1	4.0	9.4	0.5	13.5	14.5	0.7	20.8	
	Sum	457.6	100.0	-	-	-	-	-	-	-	7.5	-	-	27.5	-	30.3	164.5	
Hercynite low Fe (A)	Conventional, Jaw crusher	4-3.15	46.8	10.2	22.5	0.3	1.4	<3.63	21.3	4.3	0.9	2.2	1.6	0.3	0.9	39.1	8.4	17.9
								>3.63	0.8	12.7	0.1		10.5	0.1		16.2	0.1	
		3.15-1	221.1	48.1	42.0	0.6	1.5	<3.63	38.8	3.5	1.4	9.4	2.7	1.0	6.7	39.0	15.1	83.8
								>3.63	2.6	15.5	0.4		9.1	0.2		21.8	0.6	
		<1	191.4	41.7	5.0	-	-	-	5.0	3.6	0.2	6.9	2.9	0.1	5.6	25.8	1.3	49.4
		Sum	459.3	100.0	-	-	-	-	-	-	-	18.5	-	-	13.2	-	25.5	151.1
	Conventional, Impact crusher	4-3.15	29.8	10.4	15.0	0.3	1.7	<3.63	14.3	3.2	0.5	1.0	5.8	0.8	1.8	33.6	4.8	9.9
								>3.63	0.4	8.7	0.0		10.2	0.0		23.4	0.1	
		3.15-1	139.4	48.9	45.0	0.5	1.0	<3.63	40.5	0.8	0.3	1.2	3.2	1.3	4.7	34.5	14.0	48.9
								>3.63	4.0	2.2	0.1		5.1	0.2		41.3	1.7	
		<1	115.8	40.6	5.0	-	-	-	5.0	3.4	0.2	3.9	2.9	0.1	3.4	28.9	1.4	33.5
		Sum	284.9	100.0	-	-	-	-	-	-	-	6.2	-	2.5	9.9	-	22.0	92.3
Conventional, Cone crusher	4-3.15	22.9	8.1	20.0	0.4	1.8	<3.63	19.5	2.0	0.4	0.5	3.2	0.6	0.8	49.5	9.6	11.3	
							>3.63	0.2	15.0	0.0		15.1	0.0		16.2	0.0		
	3.15-1	120.9	42.7	48.5	0.6	1.2	<3.63	43.4	2.5	1.1	2.9	3.6	1.6	4.4	32.2	14.0	39.4	
							>3.63	4.5	1.8	0.1		4.0	0.2		36.6	1.7		
	<1	139.4	49.2	5.0	-	-	-	5.0	3.0	0.2	4.2	2.8	0.1	3.9	26.2	1.3	36.5	
	Sum	283.3	100.0	-	-	-	-	-	-	-	7.7	-	2.5	-	-	26.6	87.1	

m total [g] Mass of the particle size class from the fine fraction samples PSD
fraction [%] Mass percentage of the particle size class from the fine fraction samples PSD
m sample [g] Mass of the sample, which was used for the density tests
m loss [g] Mass of sample loss during the density trial
fraction loss [%] Mass percentage of sample loss during the density trial
Density [g/cm³] Density class in which fraction enriched after the separation process
Element (xx) [%] Mass percentage of element in the separated sample, measurement method mentioned in brackets
Element total [g] Mass of the element, which is stored in the particle size class

5 Conclusion

5.1 Coarse comminution, <120 mm

The comprehensive comminution experiments conducted at RHI Magnesita GmbH and ARP GmbH have provided valuable insights into the performance and comminution behavior of various crushing equipment for processing breakout materials from the cement and steel industries (Hercynite and MgO-C). The trials, which focused on coarse comminution of pre-crushed material (<120 mm), compared the efficiency of a jaw crusher, cone crusher, and impact crusher in achieving the desired particle size distributions and minimizing fines production.

The pre-tests revealed that the cone crusher was the most suitable equipment for the task, achieving a satisfactory particle size distribution with a low mass of the fraction <5 mm and favorable k20 and k80 values. Sample C (MgO-C) exhibited a finer comminution behavior compared to the Hercynite

samples (A and B) when employing the impact crusher, while sample B yields finer particles than sample A across all equipment types.

The particle shape analysis indicated that the cone crusher tended to produce a conchoidal shape, while the impact crusher resulted in a more cubic and compact form. This preceding analysis leads to the hypothesis, that the influence of crushing equipment on particle shape is higher than the influence of the specific material characteristic of examined refractories.

5.2 Conventional and alternate comminution, <4 mm

Electrodynamic fragmentation as alternate comminution technology

High voltage pulse power fragmentation or electrodynamic fragmentation is a novel route for the comminution to weaken or fully fragment minerals based on highly energetic electrical pulses. The high voltage breakage experiments were performed as wet batch processes. Process parameters to be adjusted are the voltage of the discharges that regulates the energy of the pulses and number of pulses.

Applying a higher voltage or higher pulse to an identical feed leads to a finer product particle size distribution. Dividing the bulk feed (5–40 mm) into several feed size classes (5–10 mm and 10–20 mm) improves the particle size distribution, where 5–10 mm feed size has the better particle size distribution and increases the energy efficiency.

The study on EDF as a comminution technology for particle liberation in spent refractory bricks has provided valuable insights into the effectiveness of this method. The experiments conducted have achieved the desired particle size reduction to less than 4 mm, which is essential for the liberation of particles in refractory materials.

The experiments revealed a notable size reduction for MgO-C. In contrast, for Hercynite, despite an increase in voltage and pulses leading to finer comminution, the k80 values did not show a significant difference between feed and product, indicating the complexity of the material's permittivity and its impact on the comminution process. The comminution of Hercynite using EDF is challenging because the size reduction of Hercynite bricks using EDF only results in a small reduction ratio. A potential explanation for this can be attributed to the electrical conductivity of water. Processing Hercynite increases the conductivity of the water more than the MgO-C does, which causes the electric beam to pass through the water instead of the sample. As a consequence, loss of the pulse energy in the water increases and results in a weak comminution of the Hercynite samples.

5.3 Fractional class analysis

In conclusion, the fractional class analysis conducted through specific gravity-based separability curves has provided a better understanding of intergrowth and processability in spent refractory bricks. The use of sodium polytungstate solution as a heavy medium, with tungsten carbide as additive for higher densities, facilitated the separation of samples into distinct density classes.

Evaluating the results, it is important to note that the elemental analysis was performed with a handheld XRF device which provides lower accuracy and precision compared to laboratory systems.

The pre-trials for the MgO-C material identified three separable densities—2.7 g/cm³, 3.0 g/cm³, and 3.5 g/cm³— which led to the creation of four density classes. The density of 3.0 g/cm³ became evident as a threshold for effectively differentiating between MgO-rich and C-rich components.

The Henry-Reinhardt (HR) diagrams served as a suitable tool for visualizing the results of the density separation trials. For the MgO-C fraction of 4–3.15 mm, originating from jaw crusher comminution, the HR diagrams revealed that Mg enrichment is apparent at densities greater than 3.0 g/cm³, with grades of 56 % and 58 % for the >3.5 g/cm³ and 3.0–3.5 g/cm³ classes, respectively.

Conversely, the carbon content showed an increase in the lighter fractions, with the HR diagrams indicating a higher carbon presence in products with densities less than 3.0 g/cm³. This aligns with the expectation that carbon would be enriched in the less dense classes.

The overall results from the MgO-C density trials indicate that, across various particle size classes, carbon can be consistently enriched in the density class below 3.0 g/cm³, while Mg enrichment is more variable, particularly for the lab-scale EDF and cone crusher technologies. The EDF technology, showed the least favorable results for Mg enrichment, whereas the jaw crusher demonstrated the highest performance in liberating particles.

In the case of Hercynite, the selected density classes of <3.63 g/cm³ and >3.63 g/cm³ were expected to yield metal-enriched fractions. However, the low contents and small masses of Fe and Al in these classes made the creation of HR diagrams unfeasible, thus preventing a thorough evaluation of the liberation across different comminution technologies.

5.4 Impact on ReSoURCE

The scope of this deliverable was to identify the most effective pre-processing method for subsequent automated sorting. The investigation found that particle shape differences were minimal across the various refractory types, and these types did not significantly differ in the features obtained. The impact crusher was considered unsuitable due to the excessive generation of fines. Conversely, both the jaw and cone crushers demonstrated comparable and acceptable performance for material preparation in Demonstrator A.

Regarding material liberation, which is crucial for subsequent refractory production and preparing material for Demonstrator B, the electrodynamic fragmentation did not yield favorable results. The jaw crusher emerged as the most effective in achieving material liberation, making it the optimal choice for the recycling process. Its performance, coupled with the advantage of being standard equipment, reinforces its suitability for this application.

6 References

- [1] Arianpour, F., Kazemi, F., and Fard, F. G. 2010. Characterization, microstructure and corrosion behavior of magnesia refractories produced from recycled refractory aggregates. In: Minerals Engineering, Volume 23, Issue 3, pp 273-276.
- [2] Schubert, H. 1989. Aufbereitung fester mineralischer Rohstoffe Band I: Kennzeichnung von Körnerkollektiven, Kennzeichnung von Aufbereitungs- und Trennerfolg, Zerkleinerung, Klassierung (In German). 3. Auflage; Leipzig: Dt. Verl. Für Grundstoffindustrie, 1989.
- [3] van der Wielen, K. P. 2013. Application of High Voltage Breakage to a Range of Rock Types of Varying Physical Properties. Dissertation, University of Exeter.
- [4] van der Wielen, K. P. 2013. The influence of equipment settings and rock properties on high voltage breakage. In: Minerals Engineering, Volume 46-47, pp 100-111.
- [5] Kong, E. 2021. Simulation of rock breaking test by high voltage electric pulse discharge based on Selfrag. In: Drilling Engineering, 2021, 48(8), pp 40-46.
- [6] Seifert, S., Thome, V. and Karlstetter, C. 2014. Elektrodynamische Fragmentierung-Eine Technologie zur effektiven Aufbereitung von Abfallströmen. In: Recycling und Rohstoffe, Band 7, TK Verlag, pp 431-438.
- [7] Königshofer, S. 2015. Research on the processing of spent magnesia-carbon refractory bricks for developing innovative recycling approaches. Dissertation. Montanuniversitaet Leoben, Chair of Mineral Processing.
- [8] Selfrag 2024. Pulse Power. <http://www.selfrag.com/technology-pulse.php>. (last requested at 06.08.2024).
- [9] Singh, K. 2017. A Geometallurgical Forecast Model for Predicting Concentrate Quality. WLIMS Process for Leveäniemi Ore. Master thesis. Lulea University of Technology, Department of Civil, Environmental and Natural Resources Engineering.
- [10] Govindarajan, B., Rao, T. C. 1994. Indexing the washability characteristics of coal. International Journal of Mineral Processing, Volume 42, Issues 3-4, pp 285-293.
- [11] Niiranen, K. 2017. Characterization of the Kiirunavaara iron ore deposit for mineral processing with a focus on the high silica ore type B2. Dissertation. Montanuniversitaet Leoben, Chair of Mineral Processing.
- [12] Metso 2024. 5 tips for energy-efficient and productive comminution with cone crushers. <https://www.metso.com/de/einblicke/blog/gesteinsindustrie/5-tipps-fur-energiesparendes-und-produktives-brechen-mit-kegelbrechern/> (last requested at 06.08.2024).
- [13] Wirtgen Group 2024. Comminution technologies. <https://www.wirtgen-group.com/de-at/produkte/kleemann/technologien/brechtechnik/> (last requested at 06.08.2024).
- [14] Terex-Finlay 2024. Crusher Wear Parts Reference Guide. https://www.terex.com/docs/librariesprovider4/spare-parts-documents/terex_finlay_crusher_reference_guide_2018.pdf (last requested at 06.08.2024).

7 List of figures

Figure 1: Principles of different comminution types [2]	6
Figure 2: Principles of jaw crusher [2]	7
Figure 3: Principles of cone crusher [2].....	8
Figure 4: Principles of impact crusher [1].....	8
Figure 5: EDF lab equipment at MUL [5]	9
Figure 6: selfFrag lab device's schematic [7]	10
Figure 7: Initial particle size distribution of cement rotary kiln breakout material (CRK1).	12
Figure 8: sample A (Hercynite), sample B (Hercynite) and sample C (MgO-C), from left to right.	13
Figure 9: Preselecting comminution equipment - Flowsheet cone crusher.	14
Figure 10: Industrial comminution equipment - Flowsheet cone crusher.....	15
Figure 11: Circular vibratory screen with two screen decks	15
Figure 12: Cone crusher in operation.....	16
Figure 13: Laboratory crushing tests – particle size classes (left: fused magnesia >20 mm, right: sintered magnesia 0–40 mm).....	16
Figure 14: Laboratory crushing tests – particle size classes (left: Hercynite 1 >20 mm, right: Hercynite 2 >20 mm)	17
Figure 15: Laboratory crushing tests – jaw crusher	17
Figure 16: Laboratory crushing tests – flow sheet jaw crusher	17
Figure 17: Simplified Henry Reinhardt chart [11].....	19
Figure 18: Sodium polytungstate solution for sink-float-analysis, density 3.00 g/cm ³	19
Figure 19: Scheme for the trials to evaluate the particle liberation for the different comminution technologies	20
Figure 20: Experimental setup for the density trials.....	21
Figure 21: Pulverisette vacuum ball mill	21
Figure 22: Analysis of particle size and particle shape distribution – particle shape slide gauge.....	22
Figure 23: Analysis of particle size and particle shape distribution – Sample A cone crusher, subsample fraction 20/10 mm	23
Figure 24: Particle size distribution of various used refractories by using jaw crusher.....	25
Figure 25: Particle size distribution of various used refractories by using cone crusher.....	25
Figure 26: Particle size distribution of various used refractories by using impact crusher	26
Figure 27: Particle shape distribution sample A (Hercynite A) using different crushing equipment....	26
Figure 28: Particle shape distribution sample B (Hercynite B) using different crushing equipment....	27
Figure 29: Particle shape distribution sample C (MgO-C) using different crushing equipment	27
Figure 30: Particle shape distribution for various types of used refractories – cone crusher (setting II)	27
Figure 31: Particle shape distribution for various types of used refractories – jaw crusher	28
Figure 32: Particle shape distribution for various types of used refractories – impact crusher (setting II).....	28
Figure 33: Product & feed particle size distribution of MgO-C 5–40 mm sample band	30
Figure 34: Product & feed particle size distribution of MgO-C 10–20 mm sample band	30
Figure 35: Effect of Voltage on Particle Size Distribution of MgO-C Product from Feed Size 5–40 mm (Constant Pulse: 60)	31
Figure 36: Effect of Voltage on Particle Size Distribution of MgO-C Product from Feed Size 10–20 mm (Constant Pulse: 60)	31
Figure 37: Effect of Pulses on Particle Size Distribution of MgO-C Product from Feed Size 5–40 mm (Constant V: 150 kV).....	32

Figure 38: Effect of pulses on Particle Size Distribution of MgO-C Product from Feed Size 10–20 mm (Constant V: 150 kV).....	32
Figure 39: Effect of voltage variation on the size distribution of the MgO-C product while operating on constant 100 pulses.....	33
Figure 40: Particle size distributions of four samples of Hercynite product of feed size 5–10 mm	34
Figure 41: Particle size distribution of four samples of Hercynite product of feed size 20 - 40 mm	34
Figure 42: Comparison of Hercynite Particle Size Distributions from feed size 5–10 and 20–40 mm at 200 kV and 100 pulses.....	35
Figure 43: Effect of MgO-C and Hercynite EDF comminution to the conductivity of the process water after 100 pulses.....	35
Figure 44: Effect of MgO-C and Hercynite EDF comminution to the pH value of the process water after 100 pulses.....	36
Figure 45: Results of the pre-trials to find suitable separation densities	37
Figure 46: HR-diagram for MgO-C Jaw crusher 4–3.15 mm of Mg grade	37
Figure 47: HR diagram for MgO-C comminuted with a jaw crusher and a particle size 4–3.15 for carbon grade	38

8 List of tables

Table 1: Particle shape distribution – sample and analysis overview	23
Table 2: Comminution characteristics for different crushing equipment and various used refractories	24
Table 3: Chemical analysis of various used refractories (samples A, B and C).....	29
Table 4: Codification of samples in the experiment.....	29
Table 5: Parameters of EDF setting correspond to energy generator, spark energy and efficiency	32
Table 6: Parameters of EDF setting correspond energy and its efficiency from 150 kV – 100 P and 200 kV – 100 P	33
Table 7: Main components of MgO-C refractory bricks with their densities.....	36
Table 8: Data of pre-trials for the determination of suitable separation densities	36
Table 9: Results for the MgO-C density trials with a heavy liquid of 3.0 g/cm ³	39
Table 10: Main components of Hercynite refractory bricks with their densities	39
Table 11: Results for the Hercynite density trials with a heavy liquid of 3.63 g/cm ³	40

9 Appendix

Results for the MgO-C density trials with a heavy liquid of 3.0 g/cm³

Refractory	Comminution technology	Particle size [mm]	m total [g]	fraction [%]	m sample [g]	m loss [g]	fraction loss [%]	density [g/cm ³]	m sample [g]	C (LECO) [%]	C sample [g]	C total [g]	Mg (XRF) [%]	Mg sample [g]	Mg total [g]	LE (XRF) [%]	LE sample [g]	LE total [g]	Further (XRF) [%]	Further sample [g]	Further total [g]	Check m total [g]	Check XRF [%]	
MgO-C	Conventional, Jaw crusher	4-3.15	44.8	9.4	32.5	0.3	1.0	<3.0	6.8	20.2	1.4	2.8	32.3	2.2	23.7	41.9	2.8	16.7	25.9	1.8	4.4	47.6	100.0	
								>3.0	25.4	2.7	0.7		58.5	14.8		36.1	9.2		5.4	1.4			100.0	
		3.15-1	205.8	43.2	42.5	0.4	1.1	<3.0	11.5	21.3	2.5	19.9	32.7	3.8	79.4	39.9	4.6	101.6	27.4	3.2	24.8	225.6	100.0	
								>3.0	30.5	5.3	1.6		40.8	12.5		52.9	16.2		6.3	1.9			100.0	
		<1	225.8	47.4	5.0	-	-	-	5.0	15.8	0.8	35.7	44.7	2.2	100.9	47.2	2.4	106.6	8.1	0.4	18.3	261.5	100.0	
		Sum	476.3	100.0	-	-	-	-	-	-	-	58.4	-	-	204.0	-	-	224.9	-	-	47.4	534.7	-	
		Conventional, Impact crusher	4-3.15	33.5	11.8	22.5	0.1	0.7	<3.0	6.4	17.6	1.1	2.5	40.7	2.6	15.9	33.8	2.2	12.8	25.5	1.6	4.9	36.0	100.0
									>3.0	16.0	3.5	0.6		49.9	8.0		39.8	6.4		10.3	1.6			100.0
	3.15-1		122.3	43.2	110.0	0.2	0.2	<3.0	27.4	21.0	5.8	10.3	30.4	8.3	43.2	50.6	13.9	50.0	19.1	5.2	29.1	132.6	100.0	
								>3.0	82.4	4.2	3.5		37.0	30.5		37.7	31.0		25.3	20.9			100.0	
	<1		127.2	44.9	5.0	-	-	-	5.0	18.2	0.9	23.2	43.2	2.2	55.0	47.3	2.4	60.2	9.5	0.5	12.1	150.4	100.0	
	Sum		283.1	100.0	-	-	-	-	-	-	-	35.9	-	-	114.0	-	-	123.0	-	-	46.1	319.0	-	
	Conventional, Cone crusher		4-3.15	39.6	13.4	18.0	0.3	1.5	<3.0	4.2	18.9	0.8	2.7	41.2	1.7	19.2	30.9	1.3	14.8	27.9	1.2	5.5	42.3	100.0
									>3.0	13.5	3.2	0.4		51.0	6.9		39.5	5.3		9.6	1.3			100.0
		3.15-1	133.7	45.4	115.0	1.4	1.3	<3.0	86.2	21.6	18.6	22.8	44.1	38.0	55.9	50.2	43.3	59.0	5.7	4.9	18.8	156.6	100.0	
								>3.0	27.3	2.8	0.8		34.8	9.5		24.7	6.7		40.5	11.1			100.0	
		<1	121.5	41.2	5.0	-	-	-	5.0	17.8	0.9	21.6	46.8	2.3	56.8	42.2	2.1	51.3	11.0	0.6	13.4	143.1	100.0	
		Sum	294.8	100.0	-	-	-	-	-	-	-	47.2	-	-	132.0	-	-	125.0	-	-	37.7	342.0	-	
		EDF Lab, 5-10 mm, sample IV	4-3.15	31.6	6.3	25.5	0.5	2.0	<3.0	9.3	18.9	1.8	2.7	39.3	3.6	13.6	30.7	2.8	12.2	29.9	2.8	5.7	34.3	100.0
									>3.0	15.7	2.4	0.4		45.5	7.1		43.5	6.8		11.0	1.7			100.0
	3.15-1		265.1	53.1	75.0	0.6	0.8	<3.0	30.0	20.9	6.3	30.4	30.0	9.0	66.1	30.1	9.0	93.3	39.9	12.0	105.6	295.5	100.0	
								>3.0	44.4	5.1	2.3		21.5	9.6		38.7	17.2		39.8	17.7			100.0	
	<1		202.8	40.6	5.0	-	-	-	5.0	16.9	0.8	34.3	38.5	1.9	78.1	40.3	2.0	81.7	21.2	1.1	43.0	237.1	100.0	
	Sum		499.5	100.0	-	-	-	-	-	-	-	67.4	-	-	157.8	-	-	187.3	-	-	154.3	566.9	-	

m total [g]	Mass of the particle size class from the fine fraction samples PSD
fraction [%]	Mass percentage of the particle size class from the fine fraction samples PSD
m sample [g]	Mass of the sample, which was used for the density tests
m loss [g]	Mass of sample loss during the density trial
fraction loss [%]	Mass percentage of sample loss during the density trial
Density [g/cm ³]	Density class in which fraction enriched after the separation process
Element (xx) [%]	Mass percentage of element in the separated sample, measurement method mentioned in brackets
Element total [g]	Mass of the element, which is stored in the particle size class
Further	All elements measured with the XRF handheld, which are not focused in this table
Check m total [g]	Check sum of the mass balance through the density test
Check XRF [%]	Check sum, if the elements measured by XRF are resulting in 100 %

Results for the Hercynite density trials with a heavy liquid of 3.63 g/cm³

Refractory	Comminution technology	Particle size [mm]	m total [g]	fraction [%]	m sample [g]	m loss [g]	fraction loss [%]	density [g/cm ³]	m sample [g]	Fe (XRF) [%]	Fe sample [g]	Fe total [g]	Al (XRF) [%]	Al sample [g]	Al total [g]	Mg (XRF) [%]	Mg sample [g]	Mg total [g]	LE (XRF) [%]	LE sample [g]	LE total [g]	Further (XRF) [%]	Further sample [g]	Further total [g]	Check m total [g]	Check XRF [%]	
Hercynite high Fe (B)	Conventional, Jaw crusher	4-3.15	25.0	12.5	22.0	0.2	0.8	<3.63	21.5	0.6	0.1	0.2	2.8	0.6	0.7	30.5	6.6	7.6	58.0	12.5	14.5	8.1	1.7	2.0	25.0	100.0	
								>3.63	0.3	8.6	0.0	0.2	7.0	0.0		16.2	0.1		58.4	0.2		9.8	0.0			100.0	
		3.15-1	142.8	71.3	61.0	0.6	0.9	<3.63	51.2	0.4	0.2	0.7	0.6	0.3	1.0	38.0	19.4	57.1	52.5	26.9	72.2	8.4	4.3	11.8	142.8	100.0	
								>3.63	9.3	0.6	0.1	0.9	0.9	0.1		51.3	4.8		39.8	3.7		7.4	0.7			100.0	
		<1	32.5	16.2	5.0	-	-	-	5.0	2.9	0.1	0.9	9.7	0.5	3.2	18.1	0.9	5.9	51.6	2.6	16.8	17.8	0.9	5.8	32.5	103.9	
		Sum	200.3	100.0	-	-	-	-	-	-	-	-	1.8	-	1.5	4.8	-	31.7	70.6	-	45.8	103.5	-	7.7	19.6	200.3	-
	Conventional, Impact crusher	4-3.15	28.1	9.9	15.0	0.3	1.9	<3.63	14.3	1.6	0.2	0.4	8.8	1.3	2.4	29.8	4.3	8.4	47.3	6.8	13.3	12.5	1.8	3.5	28.1	100.0	
								>3.63	0.4	0.7	0.0	0.4	4.5	0.0		30.6	0.1		48.8	0.2		15.3	0.1			100.0	
		3.15-1	159.6	56.4	45.0	0.5	1.1	<3.63	40.5	1.5	0.6	4.2	15.2	6.2	24.0	18.8	7.6	29.7	47.8	19.4	75.4	16.7	6.8	26.4	159.6	100.0	
								>3.63	4.0	13.8	0.6	3.1	12.9	0.5		17.3	0.7		41.3	1.7		14.7	0.6			100.0	
		<1	95.4	33.7	5.0	-	-	-	5.0	3.3	0.2	3.1	8.5	0.4	8.1	16.3	0.8	15.5	54.4	2.7	51.9	17.6	0.9	16.8	95.4	100.0	
		Sum	283.1	100.0	-	-	-	-	-	-	-	-	7.7	-	8.4	34.5	-	13.5	53.6	-	30.7	140.6	-	10.1	46.7	283.1	-
Conventional, Cone crusher	4-3.15	67.1	14.7	22.5	0.2	1.1	<3.63	22.1	1.2	0.3	0.8	3.4	0.7	2.3	46.7	10.3	31.2	41.4	9.1	27.8	7.4	1.6	5.0	67.1	100.0		
							>3.63	0.2	0.5	0.0	0.8	9.8	0.0		19.3	0.0		50.3	0.1		20.1	0.0			100.0		
	3.15-1	246.6	53.9	43.0	0.8	1.9	<3.63	37.2	1.1	0.4	2.7	4.8	1.8	11.7	45.7	17.0	112.4	41.6	15.5	102.9	6.8	2.5	16.8	246.6	100.0		
							>3.63	5.0	1.2	0.1	4.0	4.5	0.2		45.0	2.3		42.5	2.1		6.9	0.3			100.0		
	<1	144.0	31.5	5.0	-	-	-	5.0	2.8	0.1	4.0	9.4	0.5	13.5	14.5	0.7	20.8	54.8	2.7	78.9	18.6	0.9	26.8	144.0	100.0		
	Sum	457.6	100.0	-	-	-	-	-	-	-	-	7.5	-	3.2	27.5	-	30.3	164.5	-	29.6	209.6	-	5.5	48.6	457.6	-	
Hercynite low Fe (A)	Conventional, Jaw crusher	4-3.15	46.8	10.2	22.5	0.3	1.4	<3.63	21.3	4.3	0.9	2.2	1.6	0.3	0.9	39.1	8.4	17.9	47.9	10.2	22.5	7.1	1.5	3.3	46.8	100.0	
								>3.63	0.8	12.7	0.1	9.4	10.5	0.1		16.2	0.1		54.1	0.5		6.5	0.1			100.0	
		3.15-1	221.1	48.1	42.0	0.6	1.5	<3.63	38.8	3.5	1.4	9.4	2.7	1.0	6.7	39.0	15.1	83.8	46.9	18.2	104.0	7.9	3.1	17.1	221.1	100.0	
								>3.63	2.6	15.5	0.4	6.9	9.1	0.2		21.8	0.6		48.8	1.3		4.8	0.1			100.0	
		<1	191.4	41.7	5.0	-	-	-	5.0	3.6	0.2	6.9	2.9	0.1	5.6	25.8	1.3	49.4	53.8	2.7	103.0	13.9	0.7	26.6	191.4	100.0	
		Sum	459.3	100.0	-	-	-	-	-	-	-	-	18.5	-	1.8	13.2	-	25.5	151.1	-	32.8	229.5	-	5.5	47.0	459.3	-
	Conventional, Impact crusher	4-3.15	29.8	10.4	15.0	0.3	1.7	<3.63	14.3	3.2	0.5	1.0	5.8	0.8	1.8	33.6	4.8	9.9	49.3	7.1	14.7	8.0	1.2	2.4	29.8	100.0	
								>3.63	0.4	8.7	0.0	1.0	10.2	0.0		23.4	0.1		51.6	0.2		6.2	0.0			100.0	
		3.15-1	139.4	48.9	45.0	0.5	1.0	<3.63	40.5	0.8	0.3	1.2	3.2	1.3	4.7	34.5	14.0	48.9	53.2	21.5	72.9	8.4	3.4	11.6	139.4	100.0	
								>3.63	4.0	2.2	0.1	3.9	5.1	0.2		41.3	1.7		43.6	1.7		7.8	0.3			100.0	
		<1	115.8	40.6	5.0	-	-	-	5.0	3.4	0.2	3.9	2.9	0.1	3.4	28.9	1.4	33.5	50.1	2.5	58.0	14.7	0.7	17.0	115.8	100.0	
		Sum	284.9	100.0	-	-	-	-	-	-	-	-	6.2	-	2.5	9.9	-	22.0	92.3	-	33.1	145.6	-	5.6	30.9	284.9	-
Conventional, Cone crusher	4-3.15	22.9	8.1	20.0	0.4	1.8	<3.63	19.5	2.0	0.4	0.5	3.2	0.6	0.8	49.5	9.6	11.3	40.2	7.8	9.2	5.2	1.0	1.2	22.9	100.0		
							>3.63	0.2	15.0	0.0	0.5	15.1	0.0		16.2	0.0		47.0	0.1		6.8	0.0			100.0		
	3.15-1	120.9	42.7	48.5	0.6	1.2	<3.63	43.4	2.5	1.1	2.9	3.6	1.6	4.4	32.2	14.0	39.4	49.8	21.6	59.5	12.0	5.2	14.7	120.9	100.0		
							>3.63	4.5	1.8	0.1	4.2	4.0	0.2		36.6	1.7		44.0	2.0		13.5	0.6			100.0		
	<1	139.4	49.2	5.0	-	-	-	5.0	3.0	0.2	4.2	2.8	0.1	3.9	26.2	1.3	36.5	52.4	2.6	73.1	15.6	0.8	21.7	139.4	100.0		
	Sum	283.3	100.0	-	-	-	-	-	-	-	-	7.7	-	2.5	9.1	-	26.6	87.1	-	34.1	141.8	-	7.6	37.6	283.3	-	

- m total [g] Mass of the particle size class from the fine fraction samples PSD
- fraction [%] Mass percentage of the particle size class from the fine fraction samples PSD
- m sample [g] Mass of the sample, which was used for the density tests
- m loss [g] Mass of sample loss during the density trial
- fraction loss [%] Mass percentage of sample loss during the density trial
- Density [g/cm³] Density class in which fraction enriched after the separation process
- Element (xx) [%] Mass percentage of element in the separated sample, measurement method mentioned in brackets
- Element total [g] Mass of the element, which is stored in the particle size class
- Further All elements measured with the XRF handheld, which are not focused in this table
- Check m total [g] Check sum of the mass balance through the density test
- Check XRF [%] Check sum, if the elements measured by XRF are resulting in 100 %